

# A secretory form of Parkin-independent mitophagy contributes to the repertoire of extracellular vesicles released into the tumour interstitial fluid in vivo

Marissa Howard<sup>1</sup> | James Erickson<sup>2</sup> | Zachary Cuba<sup>2</sup> | Shawn Kim<sup>1</sup> | Weidong Zhou<sup>1</sup> |  
 Purva Gade<sup>1</sup> | Rachel Carter<sup>1</sup> | Kelsey Mitchell<sup>1</sup> | Heather Branscome<sup>2</sup> | Daivik Siddhi<sup>1</sup> |  
 Fatimah Alanazi<sup>1</sup> | Yuriy Kim<sup>2</sup> | Robyn P. Araujo<sup>3</sup> | Amanda Haymond<sup>1</sup> |  
 Alessandra Luchini<sup>1</sup> | Fatah Kashanchi<sup>2</sup> | Lance A. Liotta<sup>1</sup>

<sup>1</sup>Center for Applied Proteomics and Molecular Medicine, George Mason University, Manassas, Virginia, USA

<sup>2</sup>Laboratory of Molecular Virology, School of Systems Biology, George Mason University, Manassas, Virginia, USA

<sup>3</sup>School of Mathematical Sciences, Queensland University of Technology, Brisbane, Australia

## Correspondence

Marissa Howard and Lance A. Liotta, Center for Applied Proteomics and Molecular Medicine, George Mason University, Manassas, VA, USA.  
 Email: [mhowar13@gmu.edu](mailto:mhowar13@gmu.edu) (M. H.); [lliotta@gmu.edu](mailto:lliotta@gmu.edu) (L. A. L.)

## Funding information

This research study was partly supported by NIH, Grant/Award Numbers: AI078859, AI074410, AI127351-01, AI043894, NS099029; Department of Defence, Grant/Award Numbers: W81XWH-20-BCRP-BTA12, R21AI154295, R01AR068436, R33CA206937; ARC Future Fellowship Award FT190100645 to Robyn P. Araujo and NIH Department of Defence, Grant/Award Number: R21CA251015

## Abstract

We characterized the in vivo interstitial fluid (IF) content of extracellular vesicles (EVs) using the GFP-4T1 syngeneic murine cancer model to study EVs in-transit to the draining lymph node. GFP labelling confirmed the IF EV tumour cell origin. Molecular analysis revealed an abundance of IF EV-associated proteins specifically involved in mitophagy and secretory autophagy. A set of proteins required for sequential steps of fission-induced mitophagy preferentially populated the CD81+/PD-L1+ IF EVs; PINK1, TOM20, and ARIH1 E3 ubiquitin ligase (required for Parkin-independent mitophagy), DRP1 and FIS1 (mitochondrial peripheral fission), VDAC-1 (ubiquitination state triggers mitophagy away from apoptosis), VPS35, SEC22b, and Rab33b (vacuolar sorting). Comparing in vivo IF EVs to in vitro EVs revealed 40% concordance, with an elevation of mitophagy proteins in the CD81+ EVs for both murine and human cell lines subjected to metabolic stress. The export of cellular mitochondria proteins to CD81+ EVs was confirmed by density gradient isolation from the bulk EV isolate followed by anti-CD81 immunoprecipitation, molecular sieve chromatography, and MitoTracker export into CD81+ EVs. We propose the 4T1 in vivo model as a versatile tool to functionally characterize IF EVs. IF EV export of fission mitophagy proteins has broad implications for mitochondrial function and cellular immunology.

## KEYWORDS

autophagosome, autophagy, breast cancer, extracellular vesicle, mitochondria, mitophagy

## 1 | INTRODUCTION

Extracellular vesicles (EVs) released from healthy and diseased tissue interstitial fluid (IF) into the lymphatic drainage are poorly understood aspects of EV biology. EVs circulating in the lymph constitute an information highway between tissues where the lymph is a portal of entry for tissue EVs to reach the blood. EVs may not be readily able to penetrate the blood vessels surrounding the tissue (Stacker et al., 2014) due to the vessel wall's barrier function. However, lymphatic vessels have high permeability to EV-sized particles (30–5000 nm), making it likely that a high proportion of EVs shed into the IF enter the draining lymph (Stacker

This is an open access article under the terms of the [Creative Commons Attribution-NonCommercial-NoDerivs License](https://creativecommons.org/licenses/by-nc-nd/4.0/), which permits use and distribution in any medium, provided the original work is properly cited, the use is non-commercial and no modifications or adaptations are made.

© 2022 The Authors. *Journal of Extracellular Vesicles* published by Wiley Periodicals, LLC on behalf of the International Society for Extracellular Vesicles.

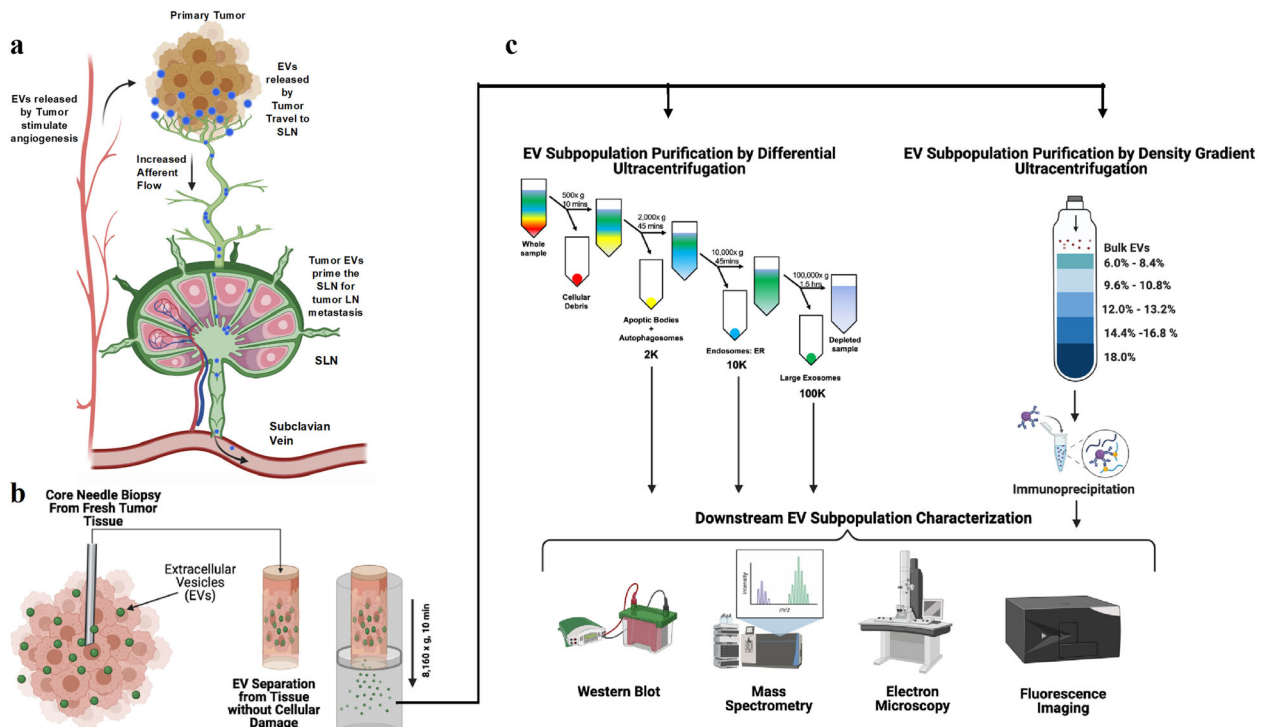


**FIGURE 1** Methodology of collecting and characterizing tumour interstitial fluid EVs. (a) Tumour cells shed EVs into the interstitial fluid (IF) of the tumour microenvironment. The IF becomes lymphatic drainage that carries the EVs to the sentinel lymph node (SLN). (b) IF resident EVs (green particles) are harvested from fresh, solid tumour tissue by low speed centrifugation. (c) Molecular characterization of EVs includes isolation and purification by differential ultracentrifugation, density gradient ultracentrifugation, and immunoprecipitation with downstream analysis by western blot, mass spectrometry, electron microscopy, and fluorescent imaging of cellular molecular tags that become EV cargo

et al., 2014) for direct delivery to the sentinel lymph node (SLN). Specifically, cancer tumour cells shed EVs over a wide range of sizes (30–5000 nm) and molecular characteristics to facilitate tumour pathogenesis, growth, immune recognition, and tumour invasion and metastasis (Lowry et al., 2015; Muller et al., 2016; Raposo & Stoorvogel, 2013; Thomas et al., 2014; Vader et al., 2014). Consequently, a high percentage of the EVs elaborated by the tumour would first encounter the innate immune system at the SLN (Figure 1a). While it has been proposed that cancer EVs can be involved in anti-apoptosis, antigen presentation, immune recognition, and immune evasion (Fleming et al., 2014; Lowry et al., 2015; Pleet et al., 2018; Vlassov et al., 2012), a majority of studies have used EVs collected from cultured cells. An understanding of the repertoire of cancer-derived EVs shed into the IF *in vivo*, and their interactions with the SLN, can provide insights into immune recognition of the tumour and into immune suppression that enables the tumour growth and metastasis (Margolis & Sadovsky, 2019; Raposo & Stoorvogel, 2013). In this study, we developed a model system to obtain a snapshot of the resident IF EVs from excised tumour tissue to elucidate the wide dynamic range of molecular characteristics and functions of IF EVs.

Previous attempts to collect tissue-derived EVs have employed organ culture or the addition of tissue damaging enzymes. Unfortunately, the EV contents released post-excision into culture media may be altered by hypoxia and physiologic shock of tissue fragment survival in the *ex vivo* environment (Gallart-Palau et al., 2016; Jang et al., 2019; Mincheva-Nilsson et al., 2016; Teng et al., 2017; Vader et al., 2014; Vella et al., 2017), and may not accurately reflect the true resident EVs within the tumour IF at the time of *ex vivo* procurement. To address these biological and technological challenges, we developed a novel method and workflow to directly isolate and enrich for EVs shed into, and existing within, the IF *in vivo* of a syngeneic tumour mass without the use of tissue extraction enzymes (Figure 1b). After validating that the IF EVs contained the cell-specific marker (enhanced green fluorescent protein (eGFP)), we further purified the EVs and density populations to evaluate their molecular cargo by mass spectrometry, western blotting, chromatography, and ultrastructural morphology (Figure 1c). To understand the importance of the global functional consequences of the separate EV categories, we studied their effects on SLN modulation of tumour growth, angiogenesis, and distant metastasis. For these functional comparisons, we employed our previously developed model of delivering isolated EVs directly in order to prime the SLN for cancer cell challenge (Longo et al., 2009; Luchini et al., 2008; Popova et al., 2015; Tamburro et al., 2011; Teunis et al., 2017).

It has been hypothesized that secretory autophagy contributes to the growth of the tumour (Dupont et al., 2011). Autophagy, “self-eating,” is a homeostatic response to degrade and recycle cellular material for energy, whereas secretory autophagy utilizes similar autophagy machinery for unconventional protein secretion (Espina et al., 2010). Secretory autophagy has never been

studied in IF (Morgan et al., 2019; New & Thomas, 2019); therefore, we studied the presence of molecular mediators specific to secretory autophagy (SEC22b and RAB33b) compared to canonical autophagy machinery (LC3-I/II and p62) (Morgan et al., 2019; New & Thomas, 2019). Further, there is a significant lack of knowledge concerning the role of cellular EV production and the mitophagy process. Mitophagy is a selective form of autophagy specifically for the removal of damaged or aged mitochondria. There are two major pathways which can induce the mitophagic process: Parkin-dependent mitophagy and Parkin-independent mitophagy (Villa et al., 2018). A majority of mitophagy research has been focused on Parkin-dependent mitophagy; however, new research has suggested that Parkin-independent mitophagy processes may play a role cancer disease progression (Villa et al., 2017). Morphologically, mitophagy is preceded by mitochondrial fission factor 1 (FIS1) triggered peripheral fission to detach end segments of mitochondria for autophagic processing (Ihenacho et al., 2021; Kleele et al., 2021). Considering mitochondrial function and energy metabolism are crucial components of normal and diseased tissue cell function, combined with the recent findings that mitochondrial proteins are present within EVs (Jang et al., 2019; Macleod, 2020), we evaluated the EVs for specific molecular complex of mitophagy. We verified our mitophagy characterization using EV density gradient separation followed by immunoprecipitation using EV specific markers followed by western blot for a key mitophagy initiator (PINK1). Additionally, we fluorescently labelled active mitochondria and tracked the fluorescent dye presence in the released EVs. The molecular characterization of the IF revealed that a specific population of EVs contained a large set of proteins all specifically associated with the sequential steps of mitophagy fission and mitophagy, not mitophagy fusion, nor mitochondria-associated apoptosis. Altogether, these results revealed a notable functional difference in the EV subpopulations, and provide new insights about the biology of secretory autophagy and extracellular mitophagy components shed within IF EVs.

## 2 | MATERIALS AND METHODS

### 2.1 | Cells

The 4T1-eGFP-Puro (Imanis Life Sciences) mammary carcinoma cell line was cultured in RPMI-1640 media (Quality Biological) supplemented with 10% heat-inactivated exosome-free foetal bovine serum (FBS) (Peak Serum), 2 mM L-glutamine (Quality Biological), 100 ug/ml streptomycin (Quality Biological), 100 U/ml penicillin (Quality Biological), and 2 ug/ml puromycin (Invivogen). The MDA-MBA-231 (ATCC) adenocarcinoma cell line was cultured in Leibovitz's L-15 (ATCC) media supplemented with 10% heat-inactivated exosome-free foetal bovine serum (FBS) (Peak Serum), 2 mM L-glutamine (Quality Biological), 100 ug/ml streptomycin (Quality Biological), and 100 ug/ml penicillin (Quality Biological) for 5 days in a flask (at 37°C and 5% CO<sub>2</sub>) before harvesting for downstream experiments. For the SLN EV immunogen priming model, the 4T1 (ATCC) mammary carcinoma cell line was cultured in RPMI-1640 (Quality Biological). When reaching confluency, cells were removed by scraping and resuspended in media after cell viability was determined by Trypan Blue exclusion.

### 2.2 | Growth of GFP-4T1 tumours and EV isolation from resident tumour interstitial fluid (IF) *ex vivo*

4T1-GFP cells at  $1 \times 10^6$ /ml were injected into the mammary fat pads of 6-week-old BALB/c mice (Charles River Laboratory). The animals were sacrificed after 4 weeks, and the tumours were excised. Following removal, the tumours were placed in an EconoSpin column lined with glass wool and suspended in 300  $\mu$ l of PBS. This assembly was then centrifuged at  $8160 \times g$  for 10 min. The flow through was harvested and then centrifugated at  $2000 \times g$  for 45 min at 4°C. The resulting “2K” pellet was harvested and the supernatant was centrifuged at  $10,000 \times g$  for 45 min at 4°C. The “10K” pellet was harvested followed by the supernatant collected and treated with nanotrap particles. Nanotrap particles (NTs) Ceres #CN1035, and Ceres #CN2010 (Ceres Nanosciences, Inc.) were used to enrich EVs from low volume, cell-free supernatant samples as previously described (Ahsan et al., 2016; Demarino et al., 2018; Narayanan et al., 2013; Pleet et al., 2016, 2018; Sampey et al., 2016). One hundred microliters of the CN1035/2010 slurry (30% CN1035, 30% CN2010 and 30% PBS) were added into the  $10,000 \times g$  depleted supernatant and allowed to rotate at 4°C overnight. The NTs were then harvested by centrifugation at  $20,800 \times g$  for 10 min at 4°C resulting in the “100K\*” pellet. These samples were later utilized in Western Blot and mass spectrometry.

### 2.3 | EV isolation by differential ultracentrifugation

The 4T1, MDA-MBA-231, and 4T1-eGFP-Puro cell cultures were grown for 5 days, after which supernatants were collected from the cultures. The supernatants were centrifugated at  $500 \times g$  for 10 min, with the resulting pellet being discarded and the resulting supernatants being collected. The supernatants were then centrifugated sequentially in a 70Ti rotor (Beckman) with the resulting pellets being saved and the resulting supernatant being used in the following centrifugations at  $2000 \times g$  for 45 min at 4°C, then

10,000 × g for 45 min at 4°C, and finally 100,000 × g for 90 min at 4°C. The resulting pellets were denoted as “2K”, “10K”, and “100K”, respectively, and were later utilized in downstream assays.

## 2.4 | Western blot analysis

Whole-cell extracts (10 µg) or concentrated differential ultracentrifuge samples (5–10 µl) were resuspended in 10 µl of Laemmli buffer, heated at 95°C for 3 min, and loaded onto a –20% Tris-Glycine SDS gel (Invitrogen). CN1035/2010 NT pellets were resuspended in 15–20 µl of Laemmli buffer then heated at 95°C for 3 min and vortexed repeating these steps three times until fully resuspended. The eluted material was then loaded onto a 4–20% Tris-Glycine gel. Gels were run at 100 V and wet-transferred overnight at 50 mA onto polyvinylidene difluoride (PVDF) membranes. Membranes were blocked in 5% milk in PBS-1X containing 0.1% Tween 20 (PBST) for a 1 h at 4°C, then incubated overnight at 4°C with appropriate primary antibody in PBST at recommended manufacturer dilutions. Antibodies used for these experiments included: anti-eGFP (Abcam), anti-CD63 (Santa Cruz), anti-CD81 (Santa Cruz), anti-CD9 (Abcam), anti-β-Actin (Abcam), anti-VEGF (Thermo Fisher), anti-LC3B (Cell Signalling), anti-p62 (Cell Signalling), anti-PINK1 (Novus Biologics), and anti-PD-L1 (Rockland). Membranes were then incubated with the appropriate horseradish peroxidase (HRP)-conjugated secondary antibody for 2 h at 4°C or for 1 h at room temperature and developed using Clarity or Clarity Max Western ECL Substrate (Bio-Rad). Luminescence was visualized on a ChemiDoc Touch Imaging System (Bio-Rad).

## 2.5 | Mass spectrometry

The EV samples (10 µl) were mixed with 20 µl of 8 M urea and reduced with 10 mM dithiothreitol at 50°C for 5 min. The mixture was alkylated with 50 mM iodoacetamide at room temperature for 15 min and digested with trypsin at 37°C for 4 h. The sample was desalted by ZipTip, dried in SpeedVac, then reconstituted with 10 µl of 0.1% formic acid for mass spectrometry (MS) analysis. Liquid chromatography coupled tandem mass spectrometry (LC-MS/MS) experiments were performed on an Exploris 480 (ThermoFisher Scientific, Waltham, MA, USA) equipped with a nanospray EASY-nLC 1200 HPLC system. Peptides were separated using a reversed-phase PepMap RSLC 75 µm i.d. × 15 cm long with 2 µm particle size C18 LC column from ThermoFisher Scientific. The mobile phase consisted of 0.1% aqueous formic acid (mobile phase A) and 0.1% formic acid in 80% acetonitrile (mobile phase B). After sample injection, the peptides were eluted by using a linear gradient from 5% to 40% B over 90 min and ramping to 100% B for an additional 2 min. The flow rate was set at 300 nl/min. The Exploris 480 was operated in a data-dependent mode in which one full MS scan (60,000 resolving power) from 300 m/z to 1500 m/z was followed by MS/MS scans in which the most abundant molecular ions were dynamically selected and fragmented by higher-energy collisional dissociation (HCD) using a collision energy of 27%. “EASY-Internal Calibration”, “Peptide Monoisotopic Precursor Selection” and “Dynamic Exclusion” (15 s duration), were enabled, as was the charge state dependency so that only peptide precursors with charge states from +2 to +4 were selected and fragmented. Tandem mass spectra were searched against the NCBI human and mouse database using Proteome Discover v 2.3 from ThermoFisher Scientific. The SEQUEST node parameters were set to use full tryptic cleavage constraints with dynamic methionine oxidation. Mass tolerance for precursor ions was 2 ppm, and mass tolerance for fragment ions was 0.02 Da. A 1% false discovery rate (FDR) was used as a cut-off value for reporting peptide spectrum matches (PSM) from the database search. For protein abundance normalization to eGFP, the mass tolerance for precursor ions was adjusted to 5 ppm, and mass tolerance for fragment ions was 0.6 Da to accommodate the post-translational modifications of eGFP.

To identify the shared proteins returned between each sample, the protein GI numbers were inputted into the web-based Venn diagram maker InteractiVenn (Heberle et al., 2015). Fold-enrichments of over-expressed protein pathways by EV sample were determined by using PANTHER pathway database (Mi & Thomas, 2009).

## 2.6 | EV-CK nanoparticle delivery synthesis

Sterile N-Isopropylacrylamide (NIPAm) particles with a ~7% molar content of acrylic acid (AAc) were synthesized by precipitation polymerization and coupled with Cibacron Blue F3G triazine dye by direct reaction between the carboxylic acid groups of the particles (Tamburro et al., 2011; Teunis et al., 2017). Cibacron Blue dyed nanoparticles (NPs) were aseptically incubated with 1 µg/ml concentration of carrier-free human CCL18/PARC (RD Systems) and 1 µg/ml of carrier-free mouse CXCL9/ MIG (Biolegend) at 4°C overnight (CK/NPs). After overnight incubation, the CK/NP mix was washed and resuspended with sterile PBS-1X. Next, the NPs were diluted 1:10 in PBS-1X and mixed equi-volume with each EV subpopulation and incubated overnight at 4°C overnight (EV/NPs). The EV/NP mix was washed and resuspended with sterile PBS-1X.

## 2.7 | Sentinel lymph node priming animal model

Six to ten-week-old BALB/c female mice were obtained from Jackson Labs. Mice were injected with 50  $\mu\text{l}$  of a 1:1 ratio of CK/NPs and EV/NP subtype via subcutaneous injection in the right foot pad. Two days later, mice were challenged with  $1 \times 10^6$  4T1 cells/mouse at the same location and monitored for spontaneous tumour growth. A control group of mice received just the 4T1 challenge. At the 4 week mark, animals were sacrificed and tissues were harvested for immunohistochemistry. Tumour growth was measured by calipers. A follow-up experiment was performed and repeated these procedures, except the treatment and tumour cell challenge were subcutaneously injected into the mammary fat pad. All animal experiments were approved by the George Mason Institutional Animal Care and Use Committee (IACUC; 1312869-1).

## 2.8 | Angiogenesis assay

To assess the effects of 4T1 EVs on tubular formation, the Angio-Ready Angiogenesis Assay System (ACS-2001-2; ATCC) was utilized. The assay was performed following the recommended protocol and experimental samples were assayed in triplicate. On day 0, the assay was initiated in fully supplemented Angio-Ready Angiogenesis Medium (ACS-2008; ATCC). On day 2, the medium was removed and replaced with a 1:2 dilution of the fully supplemented medium. Treatment with EVs was based on an approximate ratio of 1:2000 (recipient cell to EV ratio) while untreated cells received only PBS. Cells were re-treated again on day 4. A fluorescent microscope was used to image the cells at various time points and image analysis was performed using the Wimasis WimTube analysis platform.

## 2.9 | EV uptake assay

The 4T1 EVs were labelled with BODIPY 493/503 (Thermo Fisher) as per the manufacturer's protocol. Briefly, various EV samples (50–100  $\mu\text{l}$ ) were labelled for 1 h at 37°C ( $\sim 10^9 - 10^{10}$  EVs/5 $\mu\text{l}$  of dye). Samples were then passed through a Sephadex G-50 column (1 ml syringe; 0.5 ml bed volume adjusted with PBS buffer) at 2000 rpm for 2 min. The columns were washed with 25  $\mu\text{l}$  of PBS at the same speed for 2 min and the collected EVs were counted for further analysis. The unincorporated dyes were trapped at the upper 1/3 of the column and EVs were collected in the flow-through. Labelled EVs were then added to confluent cultures of ASC52telo hTERT-immortalized MSCs (SCRC-4000; ATCC). EVs were added at an approximate ratio of 1:2000 (recipient cell to EV ratio) and incubated at 37°C for a period of 6 days. Images were captured using a fluorescent microscope.

## 2.10 | Electron microscopy

EV subpopulations were imaged via transmission electron microscopy (TEM) using the in-block preparation method by Jung and Mun, with minor modifications (Jung & Mun, 2018). Briefly, pelleted EV subpopulations were fixed in 1 ml of 2.5% glutaraldehyde in 0.1 M sodium cacodylate buffer overnight at 4°C. Pellets were washed in 0.1 M sodium cacodylate, then post-fixed in 1 ml of 2% osmium tetroxide in 0.1 M sodium cacodylate buffer for 1 h at 4°C. Pellets were washed again in 0.1 M sodium cacodylate buffer then dehydrated with a graded acetone series. Dehydrated pellets were resin embedded in Spurr Low Viscosity resin (Sigma-Aldrich EM0300-1KT) via a graded series of 3:1, 1:1, and 1:3 acetone:resin, then dried overnight at 65°C in 100% resin in Beem capsules. For each EV subpopulation, 60–100 nm sections were cut on a ultramicrotome and collected on Formvar/carbon film copper TEM grids, then double stained in 2% uranyl acetate followed by Reynold's lead citrate. Sections were imaged at 200 kV on a JEOL JEM 2100-Plus.

Pooled Izon column fractions 11–15 (PINK+) were imaged via scanning electron microscopy. Sample (3  $\mu\text{L}$ ) was spotted on a silicon chip and dried under vacuum overnight. Samples were imaged uncoated on a JEOL JSM-7200F between 3 kV and 5 kV.

## 2.11 | EV Isolation by Iodixanol gradient ultracentrifugation and immunoprecipitation

Five-day-old supernatants were collected from 4T1-eGFP cells or MDA-MB-231 cells and centrifuged at 500x g for 10 min. The resulting supernatants were then incubated with ExoMax (System Biosciences) at a 1:1 ratio overnight at 4°C. After incubation, the samples were centrifuged at 2000 x g for 30 min with the resulting pellet being resuspended in 300–400  $\mu\text{l}$  of PBS. Eleven iodixanol gradient fractions (1 ml/fraction; 6.0–18.0% iodixanol with a 1.2% iodixanol increase between fractions) were created by adding iodixanol to PBS in the appropriate ratio. These fractions were then loaded into a centrifuge tube compatible with the Beckman SW41 rotor in order of highest density (18.0%) to lowest density (6.0%). This was followed by the resuspended pellet

collected from the ExoMax preparation. These samples were then centrifugated at  $100,000 \times g$  for 90 min at  $4^{\circ}\text{C}$ . The volume of the resuspended pellet and each 1 ml fraction were removed and then stored in microcentrifuge tubes. These fractions were used in various downstream assays.

Select iodixanol fractions,  $250 \mu\text{l}$ , were rotated with  $2 \mu\text{g}$  of antibody, either anti-CD81 or anti-ERCC1 (D-10) (Santa Cruz) overnight at  $4^{\circ}\text{C}$ . Samples were then incubated with  $20 \mu\text{l}$  of Protein G Plus/Protein A Agarose Suspension (Millipore Sigma) for 2 h at  $4^{\circ}\text{C}$ . These samples were centrifuged at  $15,000 \times g$  for 10 min at  $4^{\circ}\text{C}$ . The resulting pellet was then used in Western blots.

## 2.12 | Mitochondrial oxidative stress perturbation

Two 4T1-eGFP cell cultures were plated at  $10^6$  cells/ml. Untreated cells were left to grow for 5 days. Treated cells were stimulated with 10 nM of carbonyl cyanide 3-chlorophenylhydrazone (CCCP) (Sigma) and left to grow for 5 days. The supernatants were collected and EVs fractions were isolated by differential ultracentrifugation. The resulting 100K EVs were probed for anti-ARIH1 (Santa Cruz) by Western blot.

## 2.13 | Mitochondrial EV fluorescent labelling

Two 4T1-eGFP-Puro cell cultures were plated at  $10^6$  cells/ml. Untreated cells were left to grow for 48 h. Treated cells were stimulated with 10 nM and  $10 \mu\text{M}$  of CCCP and left to grow for 48 h. At 48 h, 50 nM of MitoTracker Deep Red (MTDR) (Thermo Fisher) was added to the media and left to sit overnight in the cell incubator. The supernatants were collected and EVs were isolated by differential ultracentrifugation. EVs subpopulations were plated at  $30 \mu\text{l}$  and scanned for peak emission fluorescent intensity fluorescence at 450/490 nm (absorbance/ emission) for GFP and 635/675 nm (absorbance/emission) for MTDR on a Tecan *safire*<sup>2</sup> plate reader.

## 2.14 | EV protease analysis

Tumour IF that has been depleted for 2K and 10K subpopulations by centrifugation and validated for PINK1 and CD81 positivity ( $10 \mu\text{g}$ ) were incubated with dilutions of trypsin (Promega) for 30 min at  $37^{\circ}\text{C}$ . After incubation,  $15 \mu\text{l}$  of Laemmli buffer was added to trypsin-treated and control samples. The samples were analysed via Western Blot.

## 2.15 | EV free protein separation analysis

To understand the free protein content in the EV isolation we used our previously published protocol (Pinto et al., 2021). Five-day-old supernatants were collected from eGFP-4T1 cells and centrifugated at  $500 \times g$  for 10 min, with the resulting pellet being discarded. The resulting supernatant was sequentially centrifugated to remove the 2K and 10K EV subpopulations. The resulting supernatant was then mixed with ExoMax™ (System Biosciences) at a 1:1 ratio overnight at  $4^{\circ}\text{C}$  to enrich and precipitate the EVs to reduce the free protein. After incubation, the samples were centrifugated at  $2000 \times g$  for 30 min with the resulting pellet being resuspended in  $300\text{--}400 \mu\text{l}$  of PBS. Next,  $200 \mu\text{l}$  of concentrated material was loaded onto a qEV/35 nm size exclusion column (IZON). The resulting flow through material was collected into forty  $200 \mu\text{l}$  fractions.  $100 \mu\text{l}$  of each fraction was pooled into groups of five for a total of  $500 \mu\text{l}$ . Each fraction's protein content was analysed via Bradford assay. Next, the pooled fractions were incubated overnight at  $4^{\circ}\text{C}$  with CN1035/2010 (Ceres Nanosciences). NTs were pelleted and prepared for Western blot analysis. Gel electrophoresis protein detection was performed by Silver Stain according to manufacturer instructions (Pierce Silver Stain Kit, Thermo Fisher). Densitometry analysis of the protein amount was quantified by ImageJ.

## 2.16 | Statistical analysis

Standard deviation was calculated in all quantitative experiments done in triplicate. All p-values were calculated using two-tailed Student's t-tests or one-way ANOVA as indicated. Differences were considered statistically significant when  $p < 0.05$ . All statistical analyses were performed using GraphPad Prism Software version 8.3.1.

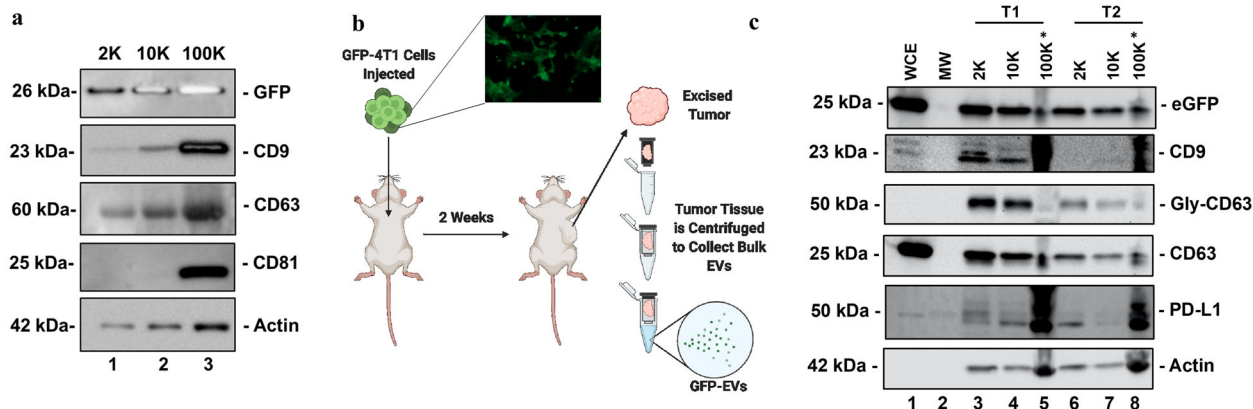


**FIGURE 2** All the major categories of IF and in vitro EVs contain the tumour cell specific eGFP marker, verifying EV tumour cell origin in vivo. (a) eGFP-4T1 mammary carcinoma cells cultured to confluency release GFP-expressing EVs into all the common EV subtypes (2K, 10K, and 100K). The GFP-expressing EVs contain specific EV markers on their surface with the highest expression levels in the 100K fraction. (b)  $10^6$  GFP-4T1 cells/ml were injected into the mammary fat pad of the syngeneic BALB/c mouse model. After 2 weeks, tumours were excised and placed in an EconoSpin column lined with glass wool and gently centrifuged at  $8160 \times g$  for 10 min to isolate bulk EVs from the tumour IF. (c) Bulk EVs isolated from the tissue were fractionated by ultracentrifugation at  $2000 \times g$  (2K) for 45 min and  $10,000 \times g$  (10K) for 45 min. Smaller diameter EVs (100K\*) were isolated via nanoparticle capture technology from the resulting 10K fraction supernatant. Expression of GFP and common EV markers were Western Blotted

### 3 | RESULTS

#### 3.1 | GFP-EVs can be harvested directly from GFP-labelled 4T1 tumour tissue

We developed a method that directly harvests the resident EVs released into the IF surrounding the tumour tissue of the 4T1 syngeneic implantable tumour model (Figure 1). To confirm the EVs collected from the fresh tissue IF were derived from tumour cells, we utilized a GFP-expressing 4T1 cell line. eGFP 4T1 cell culture-derived EVs (in vitro EVs) express GFP along with common EV tetraspanin markers, such as CD63, CD9, and CD81 (Figure 2a). The GFP brightly stains the full cell body (Figure 2b) and is exported within and density subpopulations of EVs in vitro (Figure 2a). We injected  $10^6$  eGFP-4T1 cells into the mammary fat pads (orthotopic) of the syngeneic immunocompetent BALB/c mouse model. After 4 weeks, tumours 1–2 cm were excised and immediately placed into a glass wool-packed spin column (Figure 2b). A low-speed centrifugal spin harvested the EVs from the IF gently, so the tissue sample remained histologically intact (Figure S1), with no perturbation in nuclear fine chromatic structure, cell morphology or size. A board-certified pathologist reviewed the post-EV extraction tissue compared to the non-EV extracted tissue. The 4T1 murine orthotopic tumours are highly cellular, with a high proportion of solid sheets of carcinoma cells (Pulaski & Ostrand-Rosenberg, 2000). The size and shape of the carcinoma cell body is unaltered. Furthermore, the fine nuclear chromatin, nuclear membrane and nucleoli, as well as all other morphologic elements are identical for post IF harvesting tumour tissue as compared to freshly excised intact tumours. *Ex-vivo* harvesting of resident IF and the EVs contained therein can be done in a few minutes. This includes the short time delay for low-speed centrifugation that harvests approximately 100 to 150 microliters of IF per cubic cm of tumour tissue. This time delay to centrifuge the tumour is one tenth, or less, of the earliest time to observe reactive phosphoprotein changes in *ex-vivo* tumour tissue pro-survival, hypoxia, and apoptosis pathways (Espina et al., 2008). The in vivo IF returned EVs with consistent markers for EV related tetraspanins (Figure 2c). Tumour 1 (T1) is an example of a larger tumour 1.5 cm which displayed high levels of tetraspanin markers for each EV fraction; however, tumour 2 (T2), an example of a superficial, smaller tumour, returned similar results, except that CD9 was only present in the 100K\* population. Thus, our IF-derived EV harvesting method was reliable, did not harm the tissue viability or histology, and returned enough EV sample after enrichment for subsequent orthogonal proteomic analysis.

#### 3.2 | Interstitial fluid is a rich source of EVs providing new insights into functional mechanisms

Next, we sought to understand the proteomic contents of the IF EV subpopulations. Using our high-yield mass spectrometry methodology (Magni et al., 2020), the IF EVs generated a very high content of different proteins compared to in vitro EVs (Figure 3d). Specifically, the IF EVs (*in vivo EVs*) returned over 3000 proteins for the 10K and 100K\* EV populations alone, compared to the roughly 1000 proteins returned from the in vitro EVs (Figure 3a,b). When analysing the in vitro and in vivo EV populations all together, roughly 40% ( $N = 1999$ ) of the 100K\* T1 EVs proteomic contents were unique to its populations. (Figure 3c). Indeed, the tumour microenvironment is comprised of a heterogeneous assortment of cell types including tumour

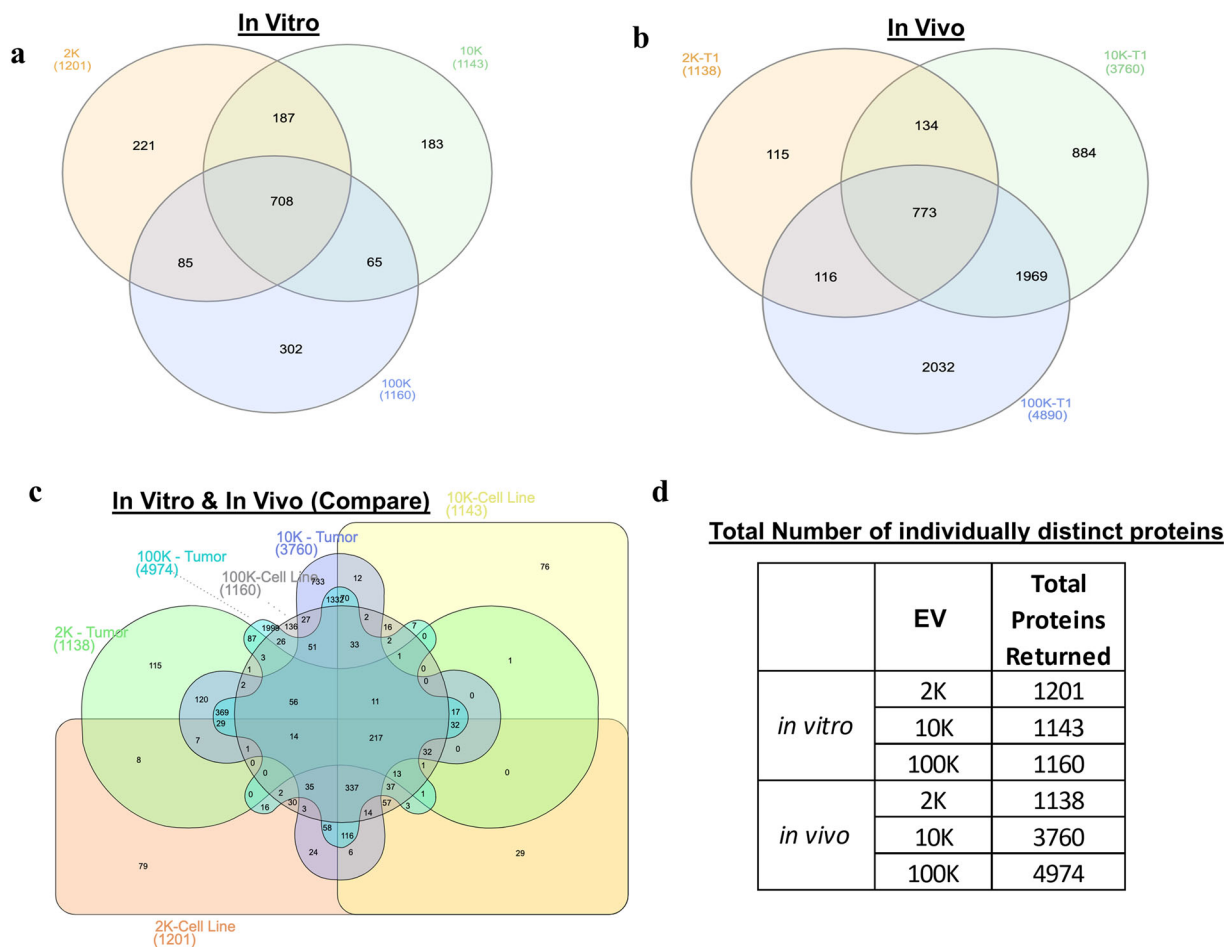


**FIGURE 3** High number and diversity of in situ IF EV cargo proteins compared to in vitro culture. (a) Culture-derived EVs were analysed by subpopulation via mass spectrometry. The proteins returned were analysed via InteractiVenn software (Heberle et al., 2015). A majority of culture-derived EVs' proteins were shared among all subpopulations. (b) Analysis of IF proteins returned from the T1 tumour show that the 10K and 100K subpopulations share a greater number of proteins than between any other set of subpopulations. The 100K EVs contained the greatest proportion and number of unique proteins. (c) Comparison of culture EVs and T1 derived EVs indicate that tumour-derived EVs of the 10K and 100K populations contain greatest number of distinct, different proteins by a factor of five. (d) Total number of in vitro versus in vivo EV proteins derived via MS demonstrate IF EVs rich repertoire of proteomic contents

cells, tumour activated fibroblasts, immune cells, collagenous stroma, muscle, fat, blood vessels, and lymphatics. The resident IF collected from any tissue volume will logically contain resident EVs that exist in the tissue at the time of the tissue excision, and the origin of such EVs will be a sampling of all the cell types in the microenvironment. While the tumour tissue studied here is a solid tumour predominated by carcinoma cells, the IF resident fluid EVs should contain important molecular information from other cell types beyond the carcinoma cells. Furthermore, lymphocytic markers are expected within IF, as it is a conduit for lymphocytic traffic. To identify the potential additional sources of non-tumour EV proteins, beyond the predominance of carcinoma cell EVs labelled with GFP, within a given IF EV subpopulation, we reviewed our proteomic data and included the protein spectrum count for proteins within our IF EVs that are non-tumour. Specifically, we reviewed IF EV subpopulation proteomic data for common normal breast epithelial (Keratin 8 and 18), basal epithelial (Keratin 5), leukocytic (CD177, neutrophil and CD5, T-cell), and tumour-activated stromal cell markers (alpha-smooth muscle actin ( $\alpha$ -SMA))(Anstine and Keri, 2019; Liu et al., 2019; Menz et al., 2021). We compared protein abundance of these cell markers to common overexpressed triple negative breast cancer marker EGFR within the same IF EV subpopulation as seen in Figure S2 (Yadav et al., 2015). As expected, relative abundance of non-tumour specific protein markers within the 100K IF EV subpopulation is significantly less than the amount of TNBC specific markers within the same IF EV subpopulation. These data demonstrate that tumour IF EVs can be a rich source of information about the functional state of all the cellular members of the tumour microenvironment. Moreover, it is important to note that tumour-activated stromal cells or cancer associated fibroblast (CAF) cells react to hypoxia by induction of autophagic flux, and can elaborate exosomes to influence the tumour microenvironment (Xi et al., 2021).

Next, we performed a head-to-head comparison by EV origin (*in vitro* vs. *in vivo*) (Figure 4). Each EV population isolated from cell culture shared a large proportion of its total protein content with the IF EVs; however, the IF EVs have a greater, more unique

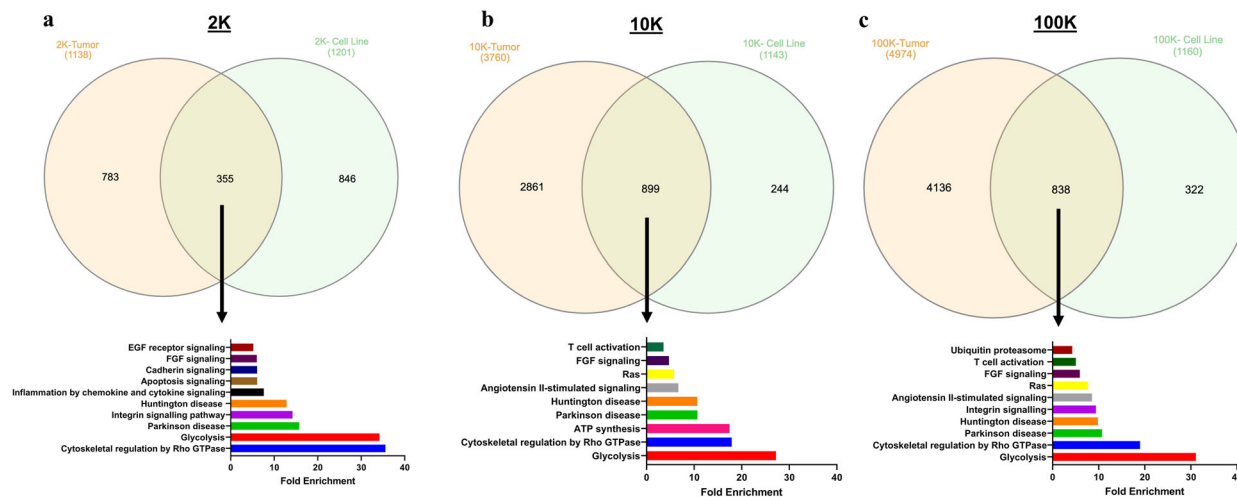


**FIGURE 4** Protein pathways analysis reveal glycolytic, neurodegenerative, and pro-angiogenic pathways are the most similar comparing in vitro to in vivo. (a) Fewer proteins are shared between the culture (green) and tumour-derived (orange) EVs for the 2K population; however, the shared pathways enriched are similar to the 10K and 100K populations. (b) 10K tumour-derived EVs contain a majority of unique peptides compared to their culture counterparts. However, the 10K and 100K EVs are both enriched for peptides associated with T cell activation and Ras pathways. (c) Similar to the 10K comparison, the 100K EVs from the tumour have a majority of unique peptides. Nevertheless, all shared pathways enriched between the EVs are indicative of neurodegenerative processes, as seen by the Parkinson's and Huntington's disease pathways, and all subpopulations are enriched for pro-angiogenic factors as seen by the fibroblast growth factor signalling pathway and angiotensin-II stimulated signalling

molecular range of proteins returned by MS. These findings suggest that EVs derived from in vitro do recapitulate many contents found in the in vivo model (generally 25% or more), particularly for the 2K and 10K populations (Figure 4a-b). We applied the PANTHER database pathway analysis to the proteins shared by each EV population in both cell culture-derived and IF-derived EVs. Each pathway represented in its analysis was significantly enriched ( $p > 0.05$ ) compared to NCBI mouse proteome. We found that the 10K and 100K EVs, regardless of origin, shared immune cell activation pathways (T-cell activation) whereas the 2K EVs shared inflammatory pathways, suggesting potential roles in immunomodulation as has been reported for EVs (Figure 4b-c) (Chen, Zhao et al., 2018b; Groza et al., 2020; Song et al., 2019). We found that EV subpopulations often had proteins indicative of pro-growth pathways such as fibroblast growth factor signalling, glycolysis, Rho-GTPase, and Ras family pathways suggesting a potential role of EVs in angiogenesis and other pro-growth survival pathways. Lastly, all EV subpopulations shared markers that are related to dysfunctional endocytic vesicle trafficking within the cell, which is typically coordinated by the degradative autophagy pathway (Wang et al., 2017). Overall, IF is a rich source of EVs with a large, dynamic proteomic output.

### 3.3 | Utility of the 4T1 model to investigate functional EV differences for Sentinel Lymph Node (SLN) immune priming

The proteomic similarities *between in vivo IF versus in vitro EV* subpopulations raises the question as to whether the subpopulations of EVs in the 4T1 model have a differential impact on the host immune recognition process occurring in the downstream SLN. Of note, the CD81+/CD63+/CD9+ 100K\* IF EVs have a high programmed death ligand 1 (PD-L1) content (Figure 2c). It has been hypothesized that PD-L1+ EVs promote tumour growth by immune suppression through the presence of PD-L1 on their surface (Chen, 2018b; Poggio et al., 2019; Song et al., 2019). Following up on this potential mechanism of tumour immune modulation, we evaluated the utility of the 4T1 model to use EV IF findings of the present study to test EV functional roles in tumour immunology. As shown in Figure S4, we compared the in vivo immunogenicity between the 100K and the 2K EVs. This experiment was modified from a previously established immunocompetent animal model to overcome the immune suppression of a *B. anthracis* infection at the SLN (Popova et al., 2015; Teunis et al., 2017). The model utilizes hydrogel nanoparticles (NPs) pre-loaded with immune chemoattractant proteins (CKs), such as CCL18/PARC and CXCL9/ MIG, as a carrier to direct pre-loaded EV subpopulations. The dual action immunization deposits EVs and CK releasing NPs to the SLN subcapsular sinus with high yield. The purpose was to recruit immune cells to recognize the simultaneously injected EVs (Figure S1a). After 48 h,  $10^6$  4T1 cancer cells/ml were injected at the same site (Figure S1b). The 100K EV treatment in this feasibility study was associated with a reduction in tumour growth and distant metastasis (Figure S4c-h), suggesting that pre-treatment with CK/100K-EV/NPs potentially primed the immune system to overcome PD-L1-mediated suppression. In contrast, the 2K EV treatment dramatically induced tumour growth and distant metastasis compared to the control group (4T1 cancer cells alone) (Figure S1c-h). One

**TABLE 1** Key functional roles of proteins returned by subtype from the T1 tumour

	Protein	Function	Presence			Reference
			2K	10K	100K	
	Fibroblast growth factor receptor 3	Common Angiogenic activator	0	0	1	Pircher et al., 2011
	Hepatoma-derived growth factor-related protein 3	Pro-angiogenic factor	0	1	1	Leblanc et al., 2015
	Annexin II	Exosomal Annexin II has been associated with increased angiogenesis and ECM remodelling, and increased metastasis	1	1	1	Maji et al., 2017
	Tumour necrosis factor alpha-induced protein	Exosomal Pro-inflammatory cytokine which increases immune cell activation to aid in cancer growth, invasion, and metastasis	0	0	1	Othman et al., 2019
<b>Inflammation, angiogenesis, and immune activation</b>	CD44	Important cancer cell signalling protein involved in stimulated angiogenesis, metabolic shift, and cancer cell proliferation.	0	1	1	Chen et al., 2018a
	High mobility group protein B2	Damage associated molecular pattern molecule which has been noted to induce autophagy and affect mitophagy	0	1	1	Tang et al., 2010
	Programmed death ligand 1 (PD-L1)	Cancer cell surface expression check-point leads to immunosuppression of emerging cancer	0	0	1	Poggio et al., 2019
	Mitogen-activated protein kinase 1 (MAPK)	Pro-cancer kinase which induces cell proliferation and growth	0	0	1	Mashouri et al., 2019
	E3 ubiquitin-protein ligase NEDD4	Ubiquitin ligase which assists LC3 in autophagosome biogenesis	1	1	1	Sun et al., 2017
	Sequestosome-1	Key autophagy substrate that targets molecules for autophagy.	0	1	0	Katsuragi et al., 2015
	Ras-related protein Rab-3D	Involved in autophagosome biogenesis	0	0	1	Morgan et al., 2019
	Ras-related protein Rab-33B	Key autophagic trafficking GTPase. noted to regulate/control exophagic viral release in HBV	0	1	1	Morgan et al., 2019
<b>Autophagy</b>	Ras-related protein Rab-4A	Overexpression of Rab-4a leads to formation of autophagosome	0	0	1	Morgan et al., 2019
	Ras-related protein Rab-1A	Aids in ULK1 translocation	1	1	1	Morgan et al., 2019
	Ras-related protein Rab-5C	Promotes ATG5-ATG12 conjugation and therefore autophagosomal elongation	0	0	1	Morgan et al., 2019
	Ras-related protein Rab-2A	Aids in autophagosome clearance	0	0	1	Morgan et al., 2019
	Vesicle-trafficking protein SEC22B	Trafficking protein involved in IL-1B secretory autophagy	0	1	1	Dupont et al., 2011

The T1 tumour EV subpopulations were analysed together using Proteome Discoverer software with the NCBI Mouse proteome database. A selected group of proteins for enriched pathways (Inflammation; Angiogenesis and Immune Activation and Autophagy) were grouped. Heatmap presence visualization demonstrates which markers for the selected proteins are in which EV subfraction.

component of this functional difference could be related to the concentration of pro-angiogenic pathways (Chiba et al., 2018; Madu et al., 2020; Pircher et al., 2011) within the 2K EVs (Figure 4a). The MS data revealed that IF EVs contained markers for angiogenesis, specifically Annexin II and hepatocyte growth factor (Table 1 – Inflammation, Angiogenesis, & Immune Activation) (Leblanc et al., 2015; Liu & Hajjar, 2016; Maji et al., 2017). To better understand the angiogenic propensity of the EVs, we applied the cell culture EVs to an in vitro angiogenesis co-culture system using hTERT immortalized mesenchymal stem cells and immortalized aortic endothelial cells and let them incubate for 6 days. After 3 days, phase contrast microscopy revealed higher levels of spheroid formation on the cells treated with 2K EVs; furthermore, after 6 days, the cells treated with the 2K EV

population had not only significantly increased tubular formation, but remarkably increased cell-to-cell contacts and branching (Figure S5a-c). We further probed these cell culture-derived EVs for vascular endothelial growth factor (VEGF), a major pro-angiogenic signalling protein, via Western Blot and found that the 2K population expressed higher levels than the 10K and 100K EV populations (Figure S5d). These *in vivo* and *in vitro* 4T1 data show how the model system proposed in the present study can go back and forth between *in vivo* and *in vitro* to pursue questions relevant to EV biology based on the striking molecular differences within the IF EV subpopulations.

### 3.4 | Secretory autophagy is a major contributor to the repertoire of IF EVs

The proteomic data returned from the IF EV subpopulations revealed an unexpectedly high content of markers associated with autophagy. Specifically, a variety of Ras-related proteins in brain (Rab) GTPases specific for aiding in the regulation of autophagosome biogenesis, trafficking proteins, and clearance proteins specific to the degradative autophagy pathway (Table 1 – Autophagy) (Morgan et al., 2019) was found. These Rab proteins were found in all EV subpopulations with increasing frequency within the 100K population. Growing evidence has indicated that EVs can be released via secretory autophagy pathway in the form of an autophagosome (Dupont et al., 2011). The MS data returned Rab-33b, a major regulator of autophagy which has been shown to be required in the release of Hepatitis B virus capsid by secretory autophagy (Morgan et al., 2019). Additionally, the molecular trafficking protein SEC22 homolog B (SEC22b), another indicator of a secretory autophagy (New & Thomas, 2019), was found in the 100K IF EVs. Next, we further probed these vesicles via Western Blot for key autophagosome markers such as microtubule-associated proteins 1A/1B light chain 3B (LC3) and sequestome 1/ p62 (Mizushima & Yoshimori, 2007; Yoshii & Mizushima, 2017). Our *in vitro* EVs demonstrated increasing intensity levels of LC3-II and p62 from 2K to 100K population (Figure 5a). The presence of LC3-II rather than LC3-I indicates a fully formed autophagosome due to the lipidation of LC3-I by phosphatidylethanolamine. The lower intensity levels seen in the 2K population of LC3-II, without the presence of LC3-I, potentially shows the initiation of LC3-II degradation rather than lack of autophagosome accumulation (Mizushima & Yoshimori, 2007; Yoshii & Mizushima, 2017). p62 is a substrate for autophagy found within the autophagosome (Katsuragi et al., 2015). Therefore, lower intensity values after immunoblotting indicate the degradation of the contents within the autophagosome. Likewise, the IF EVs for both tumours T1 and T2 demonstrated the same pattern of LC3 and p62 partial autophagosome degradation in the 2K population and autophagosome accumulation within the 100K population (Figure 5b).

A central indicator of an autophagosome is a double membrane (Ekelinin, 2005, 2008; Yoshii & Mizushima, 2017). We imaged the *in vitro* EV via transmission electron microscopy (TEM) (Figure 5c, Figure S7). For the 2K population, we found a very heterogeneous population of vesicles with varied sizes (roughly 1–5  $\mu\text{m}$ ) and visible subvesicular contents within the larger vesicular body, with varied electron densities. The 2K population has many visible vesicles within a central vesicle as seen by the darker more electron dense regions, indicative of partially degraded material (Ekelinin, 2005, 2008). These visual results show that the 2K population is more likely a collection of multivesicular bodies (MVBs) that have initiated the degradative process of autophagy, colloquially known as an amphisome (Ekelinin, 2005, 2008; Patel et al., 2013; Sanchez-Wandelmer & Reggiori, 2013). The 10K population contained varied vesicular sizes ranging from 0.5–1  $\mu\text{m}$ , but without as many clear subvesicular structures as the 2K (Figure 5c). Most of the 10K bodies appear visually lucent, therefore it is unclear whether this EV is either an autophagosome, an empty vacuole, or potentially a vesicle containing further degraded material. In contrast to the larger sized EVs, the 100K population TEM exhibited a vesicular population that was highly homogenous by size (approx. 100 nm), and morphology. Each vesicle displayed an autophagosome-like clear double membrane and dense interior content (Figure 5c, Figure S7). These data emphasises that each EV contains autophagosomes within their population that are secreted rather than degraded. Moreover, the results suggest that EV subpopulations represent different members of the autophagy pathways where the 2K EV population represents an amphisome-like population and the 100K population represents fully mature, non-degraded autophagosomes.

### 3.5 | A complete set of Parkin-independent mitophagy proteins is associated with IF EVs

A further unexpected finding in the IF EVs was a complete repertoire of fission-associated Parkin-independent mitophagy proteins. Specifically, the IF 100K\* EVs contain several E3 ubiquitin ligases implicated in Parkin-independent mitophagy: Ariadne RBR E3 Ubiquitin Protein Ligase 1 (ARIH1); HECT, UBA And WWE Domain Containing E3 Ubiquitin Protein Ligase 1 (HUWE1) (Melino et al., 2019); and Smad ubiquitin regulatory factor 1 (SMURF1) (Villa et al., 2018) as shown in Table 2 – E3 Ubiquitin ligases. In addition, the IF 100K\* EVs contain mitochondrial fission markers such as dynamin-1 like protein (DRP1) and mitochondrial fission protein 1 (FIS1), both of which have been noted to regulate the cleaving of damaged mitochondria in a fission-mediated mitophagy pathway (Table 2 – Fission Initiated) (De Paepe, 2012; Roberts et al., 2016; Villa et al., 2017, 2018; Yoon et al., 2003). These results represent a sequential record of the stages of Parkin-independent mitophagy. Next, we probed the EV subpopulations for PINK1 via Western Blot. The mitophagy pathway is initiated when PINK1 can no longer be processed by the protease PARL (Presenilins-associated rhomboid-like protein) leading to PINK1's accumulation on the outer

**TABLE 2** IF EVs contain markers for Parkin-independent mitophagy

Pathway	Sub-pathway	Protein	Function	Presence			Reference
				2K	10K	100K	
		Voltage-dependent anion-selective channel protein 1	Outer membrane mitochondrial metabolic porin that functions as a receptor for pro- and anti-apoptotic proteins.	0	1	0	Camara et al., 2017; De Paepe, 2012
		Mitochondrial import receptor subunit TOM20	Translocase which imports proteins into the intermembrane space as well as dimerizes with PINK1 under mitochondria stress to facilitate mitophagy.	0	0	1	Rasool et al., 2022
<b>Mitochondria</b>		Mitochondrial import receptor subunit TOM34	Co-chaperone of HSP70 and HSP90 involved in mitochondrial protein import.	0	0	1	Faou & Hoogenraad, 2012
		Hsp90 co-chaperone Cdc37	Chaperones involved in ULK1 complex stabilization and activation	1	1	1	Tang et al., 2010
		Vacuolar protein sorting-associated protein 35	Controller of retrograde trafficking of cargo proteins from the endosome to the trans-Golgi network. Specifically, involved in mitochondria-derived vesicle formation and mitochondrial fission.	0	1	1	Braschi et al., 2010; Cuttillo et al., 2020; Roberts et al., 2016

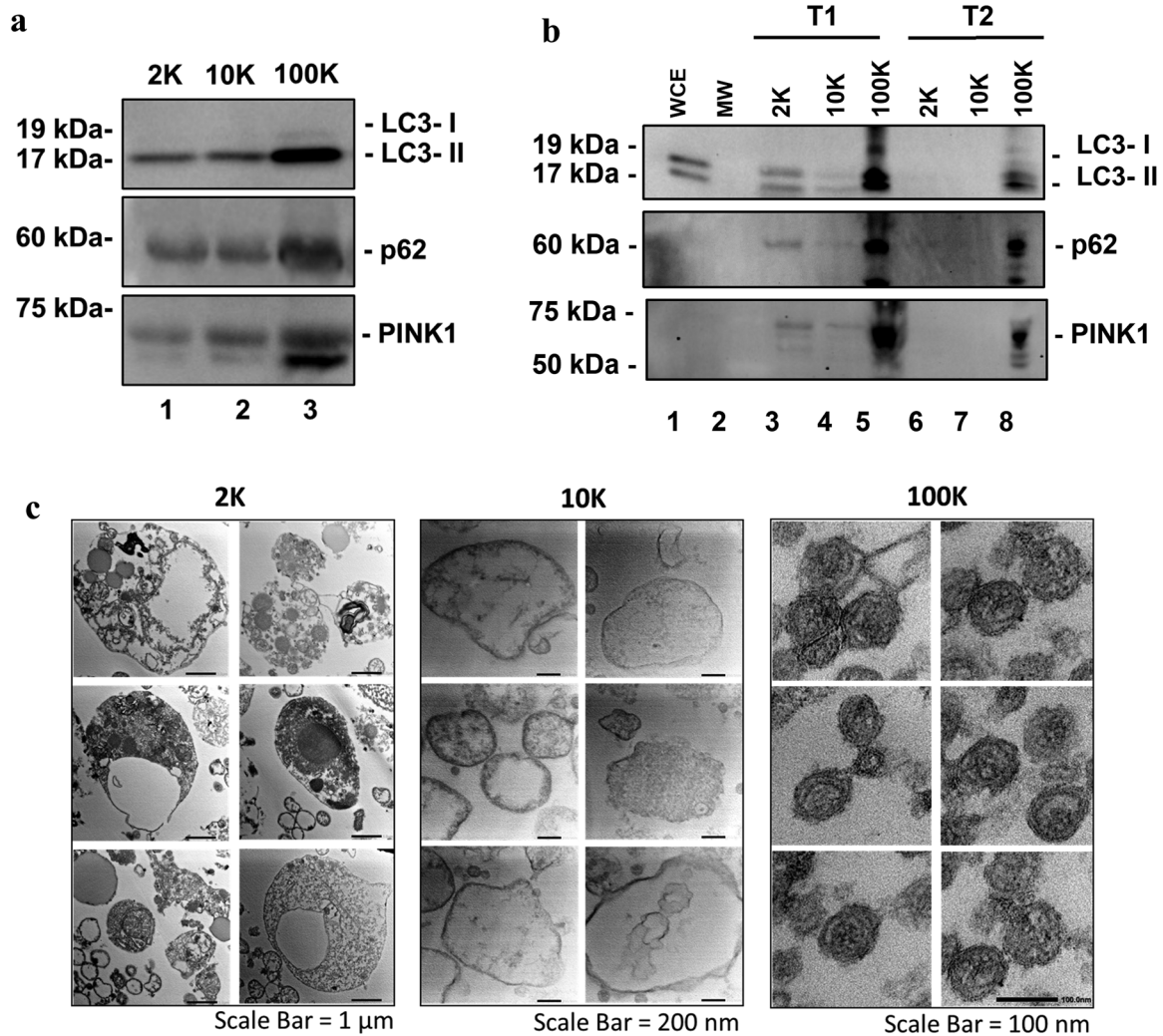
(Continues)

TABLE 2 (Continued)

Pathway	Sub-pathway	Protein	Function	Presence			Reference
				2K	10K	100K	
<i>Parkin-dependent</i>		PTEN-induced putative kinase 1 (PINK1)	Mitochondrial depolarization causes PINK1 to accumulate on the outer membrane to phosphorylate ubiquitin to Ubiquitin ligases to the mitochondrial outer membrane	1	1	1	MacLeod, 2020
	Receptor-mediated mitophagy	N.F.					Villa et al., 2018
	Lipid-mediated mitophagy	N.F.					Villa et al., 2018
<i>Parkin-independent</i>		E3 ubiquitin-protein ligase SMURF1	Regulator of mitophagy which localizes on the outer membrane to trigger autophagy machinery to damaged mitochondria	0	0	1	Melino et al., 2019
		E3 ubiquitin-protein ligase HUWE1	Inducer of AMBRA1 mediated mitophagy	0	0	1	Di Rita et al., 2018; Melino et al., 2019
		E3 ubiquitin-protein ligase ARIH1	Parkin-independent mitophagy regulator activated by PINK-1 phosphorylation to initiate p62 induced mitophagy	0	0	1	Villa et al., 2017, 2018
		mitochondrial fission 1 protein (FIS1)	Mitochondrial protein involved in fragmentation process associated with organelle fission or mitophagy	1	0	1	De Paepe, 2012
		dynamamin-1-like protein (DLPI)	GTPase enzyme that defines mitochondrial fission location with FIS1 to form a constricting ring-like structure.	1	0	1	Roberts et al., 2016; Yoon et al., 2003
Mitochondria	Peripheral Fission	mitochondrial fission factor (MFF)	Protein which initiates mid-zone mitochondrial fission.	0	0	0	Kleele et al., 2021
	Midzone Fission	dynamamin-1-like protein (DLPI)	GTPase enzyme that defines mitochondrial fission location with FIS1 to form a constricting ring-like structure.	1	0	1	Roberts et al., 2016; Yoon et al., 2003

The T1 IF EV subpopulations were analysed together using Proteome Discoverer software with the NCBI Mouse proteome database. The analysis revealed an unexpected presence of mitochondrial markers associated with a select pathway of mitophagy (Parkin-independent mitophagy). Specifically, the sub-pathways of E3 Ubiquitin Ligase and Fission Initiated Mitophagy were enriched in the 100K EV subtype.

Abbreviation: N.F., not found.



**FIGURE 5** IF EVs and in vitro EVs exhibit characteristics of autophagosomes and mitophagy by TEM and Western Blotting. (a) Western Blot analysis of culture-derived EVs reveal secreted autophagy and mitophagy related structures within all EVs. The presence of LC3-I/II and p62 indicate that these EVs are autophagosomes. Moreover, PINK-1 is the central initiator of the mitophagy process additionally found in the EVs. (b) Tumour-derived EVs confirm the results of the culture EVs and further indicate that the EVs released are involved in the secretory autophagy and mitophagy process. (c) Transmission Electron Microscopy of culture 4T1 EV subpopulations visualizes classical autophagosome characteristics such as double-membraned vesicles with internal contents for each subpopulation. By population, the 2K EVs display a heterogenous population with internal vesicle structures, and the 100K EVs are homogenous in size and structure

membrane of the mitochondria. PINK1 forms a dimer with (TOM20) and this contributes to sequestering of the full length form of PINK1 onto mitochondria targeted for mitophagy. For the EVs within the tumour IF, we verified that PINK1 and TOM20 were found together in the same EV subfraction (Figure S9a) and that the levels of the two proteins were correlated, in keeping with the expected dimerization. The accumulation of full length PINK1 will initiate an E3 ubiquitin ligase to recruit the autophagy machinery, such as p62 and LC3, to enclose the organelle within an autophagosome. For both in vivo and in vitro EVs, PINK1 and TOM20 was preferentially found in the 100K population (Figure 5a,b, Figure S9a).

The biological process of EV export of Parkin-independent and fission-associated mitophagy specific proteins was not limited to one cell type. Human triple-negative breast cancer MDA-MB-231 EV subpopulations were isolated by differential ultracentrifugation and probed for tetraspanin and autophagy markers (Figure 6a). The distribution of EV markers were similar between the eGFP-4T1 EVs and the MDA-MB-231 EVs. Similar to the mouse EVs, the 100K population of human MDA-MB-231 breast cancer cell EVs are enriched for PD-L1. The human breast cancer EVs also exhibit autophagosome properties as seen by the presence of p62 and LC3-II. The 100K population contains a large amount of p62 which would indicate a complete, undigested secreted autophagosome. Based on these similarities, we sought to identify the density fraction that would contain PINK1. Using an iodixanol density gradient we identified that PINK1 was present at lower densities (6.0%–14.4%) (Figure 6b). Next, we selected for the specific densities (9.6%–13.2%) that have been reported to contain the 100K differential ultracentrifugation population of

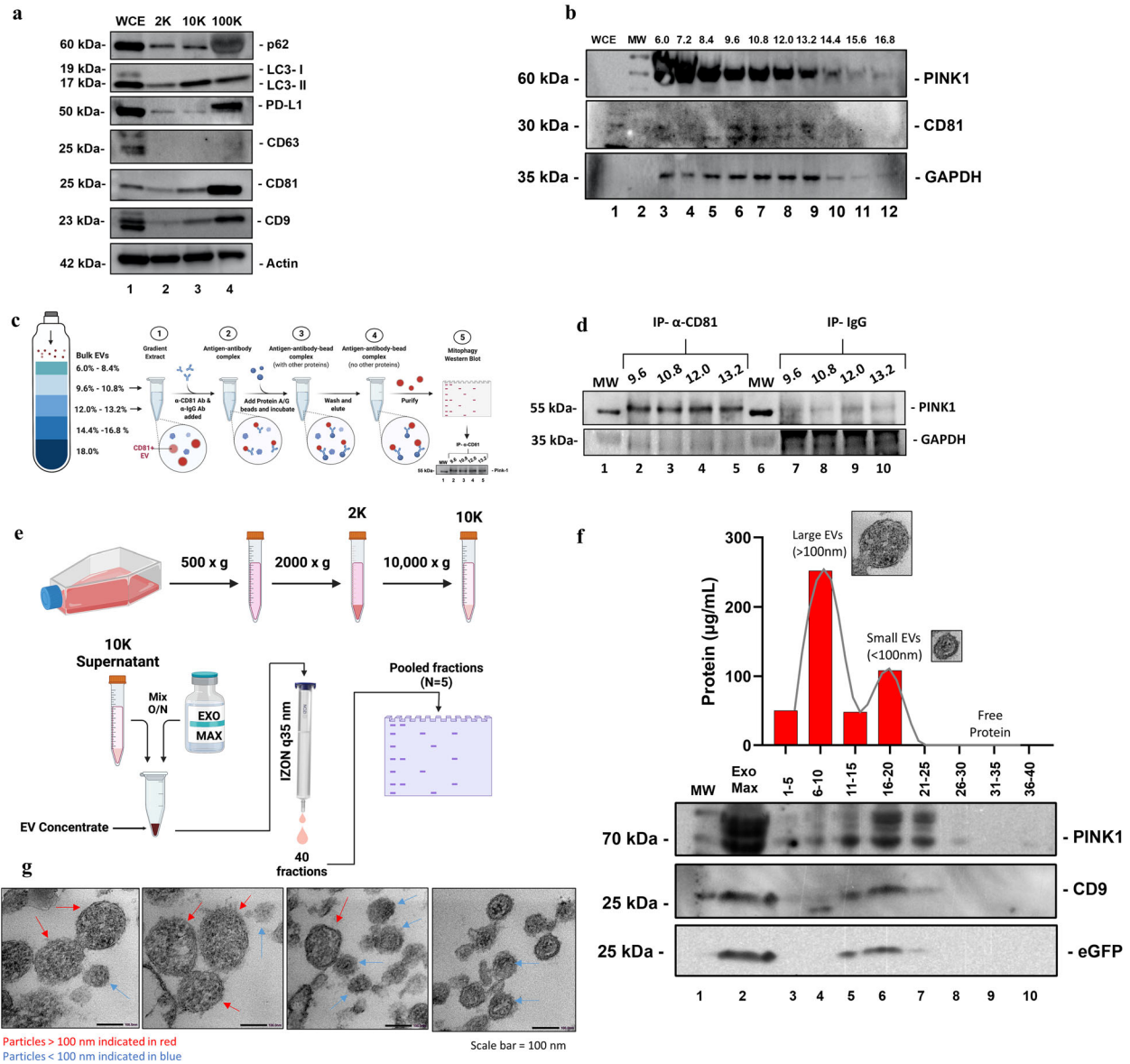


**FIGURE 6** EV subpopulation localization of key autophagy, mitophagy, and checkpoint markers. (a) Autophagosome specific p62, LC3-I/II, and checkpoint inhibitor PD-L1 are localized to the 100K CD81-enriched EVs. (b) Density gradient fractions reveal co-localization of PINK1 and CD81. (c) Immunoprecipitation of CD81+ EVs after density gradient ultracentrifugation were probed for Western Blot. (d) Anti-CD81 immunoprecipitated EVs were enriched in PINK1. (e) Five-day-old eGFP cultures were collected and differentially centrifuged to remove the 2K and 10K populations. The resulting supernatant was mixed with ExoMax solution to enrich for EVs and exclude free protein from the sample. Furthermore, to isolate the separate EV populations within the ExoMax EV concentrate, the sample was placed onto an IZON 35 nm size exclusion column. The resulting fractions were pooled into sets of 5, Nanotrapp, and analysed by Western blot. (f) The proteomic content of each set of pooled fractions found two distinct groups of EV populations (fractions 6–10 and fractions 16–20). Western blot for PINK1 revealed that this marker was preferentially within the 16–20 fraction group enriched in 35–50 nm EVs and tracked with CD9 and eGFP. (g) TEM images of eGFP-4T1 100K EVs contained two distinct populations of larger EVs (> 100 nm, red) and smaller EVs (< 100 nm, blue) by TEM

“large 100K exosomes” via immunoprecipitation (IP) with anti-CD81 (Figure 6c). The IP confirmed that the CD81+ EVs derived from the human MDA-MB-231 cell line contained the critical mitophagy marker for PINK1 (Figure 6d).

Regarding the potential contribution of free proteins (not associated with EVs) that influence the signal of mitophagy-related PINK1 found in the 100K\* pellet, we used size exclusion chromatography (Demarino et al., 2018, 2019) to assess whether the important mitochondrial proteins observed in this EV subpopulation existed in the solution phase (Figure 6e). This chromatography method successfully separates free proteins from the EVs, as show in Figure 6f, and enriches for two potentially distinct EV subpopulations (see example TEM images of Figure 6g). The results indicate that PINK1, eGFP, and CD9 were associated with smaller 35–50 nm EVs (fraction 16–20, Figure 6f), and that the fractions of free proteins were devoid of these same proteins. This

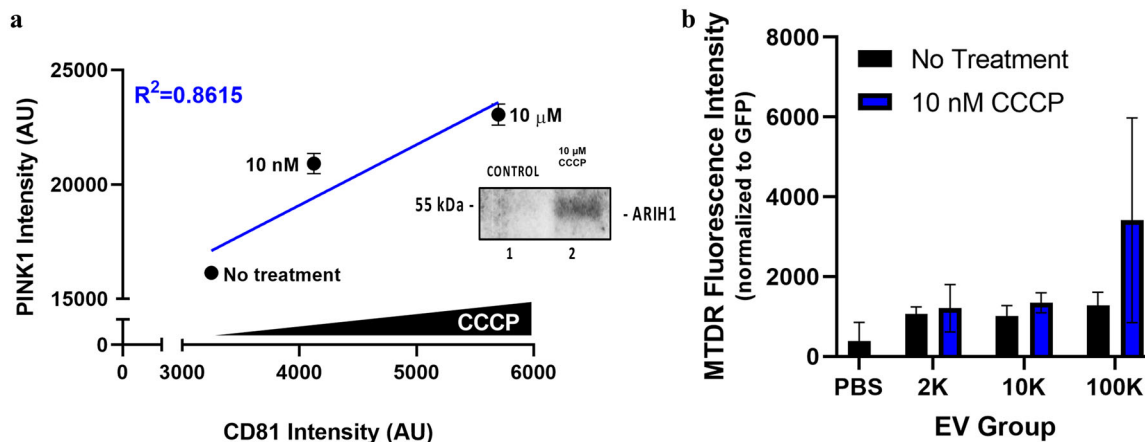


**FIGURE 7** Mitophagy induction of eGFP 4T1 EVs by CCCP correlates with PINK1 expression. (a) GFP-4T1 cells treated with increasing levels of CCCP lead to a release of increased Parkin-independent mitophagy-containing 100K EVs (ARIH1+/PINK1+/CD81+). (b) Inducing mitophagy (10 nM CCCP) within sub confluent eGFP-4T1 cells that are labelled with the mitochondrial membrane fluorescent tag MitoTracker Deep Red (MTDR) lead to an increased release of 100K EVs containing active mitochondrial molecules. MTDR fluorescence intensity was normalized to GFP fluorescence intensity by EV subpopulation

enrichment and precipitation method was further validated to demonstrate a population of PINK1 EVs (Gly-CD81+, CD81+, and Alix+) are not associated with the free protein region of the column by western blotting and imaging by SEM (Figure S10).

To further verify that PINK1-associated EVs contained mitochondrial components via a orthogonal methods, we performed a functional perturbation in vitro to induce the cellular release of mitophagy-associated EVs. We treated sub-confluent eGFP-4T1 cells with a mitochondrial depolarization protonophore carbonyl cyanide m-chlorophenyl hydrazone (CCCP) (Villa et al., 2017) and added a permanent fluorescent label for active mitochondrial membranes with MitoTracker Deep Red (MTDR) (Chazotte, 2011). After 48 h, the cells reached 70% confluency and were harvested by differential ultracentrifugation. We found that increasing CCCP to a cytotoxic level (10 µM CCCP) lead to increased release of CD81+/PINK1+ 100K EVs in a dose dependent manner (Figure 7a). We verified that the treatment of CCCP induced ARIH1 presence in the 100K EVs compared to no treatment as well (Figure 7a). The presence of MTDR was found in all EV subpopulations with increasing levels in the CCCP-treated 100K EVs (Figure 7a). We correlated these findings with GFP and found that regardless of treatment status, GFP was released consistently in all EV subpopulations (Figure 7b). Additionally, MTDR found within the EVs separately confirms that active mitochondrial components can be secreted into EVs by inducing cellular mitophagy. These data provide independent evidence of transfer of mitochondrial molecules of the Parkin-independent pathway into specific EV subpopulations, particularly under metabolic stress. We conclude that the general biological class of mitophagy protein enriched EVs are a reflection of internal mitophagy or metabolic stress that is not limited to species (murine vs. human). This implies that a more general type of EV mechanism that contains critical machinery for mitophagy exists for the removal of damaged or excess mitochondrial components (Figure 8).

## 4 | DISCUSSION

EVs shed from cells embedded within the complex in vivo tissue microenvironment passively enter the interstitial space of the tissue where they are swept into the adjacent interstitial fluid (IF). The tissue IF samples from various tissue regions merge with the lymphatic drainage for downstream filtration and immune cell examination within the local sentinel lymph node (SLN)(Figure 1a). A portion of the EVs that enter the SLN continue on to be captured in the venous drainage and ultimately enter the general blood circulation. Despite the critically important biologic role of EVs shed into tissue IF, the molecular composition, function, and traffic of EVs from tissue into the lymphatic drainage through the IF are very poorly understood (Stacker et al., 2014). We set out to develop a model system for use by the general EV community to study tissue IF EVs in a murine immunocompetent model. We employed a transplantable tumour model because we could verify that the IF EVs were derived from the tumour cells in vivo by using GFP-labelled 4T1 murine syngeneic breast cancer cells. This metastatic tumour is a murine model of human triple-negative breast cancer. An advantage of this model is that we can readily culture the 4T1 tumour cells in vitro in order to compare in vivo IF versus in vitro molecular differences in EV composition. Moreover, we can use insights from the EV molecular characterization of tumour tissue IF to pose experimental questions that employ the matched tumour cells in vitro first and can be subsequently reviewed by the in vivo model. Instead of attempting to dissociate and culture *ex vivo* tumour tissue to collect IF EVs, which could drastically alter the EV composition from that existing in situ, we gently harvested the resident IF EVs present in the tumour tissue immediately at the time of *ex vivo* tissue procurement by low speed centrifugation (Figure 1b). This did not perturb the tumour cytomorphology and did not induce tumour cell death (Figure S1). We then

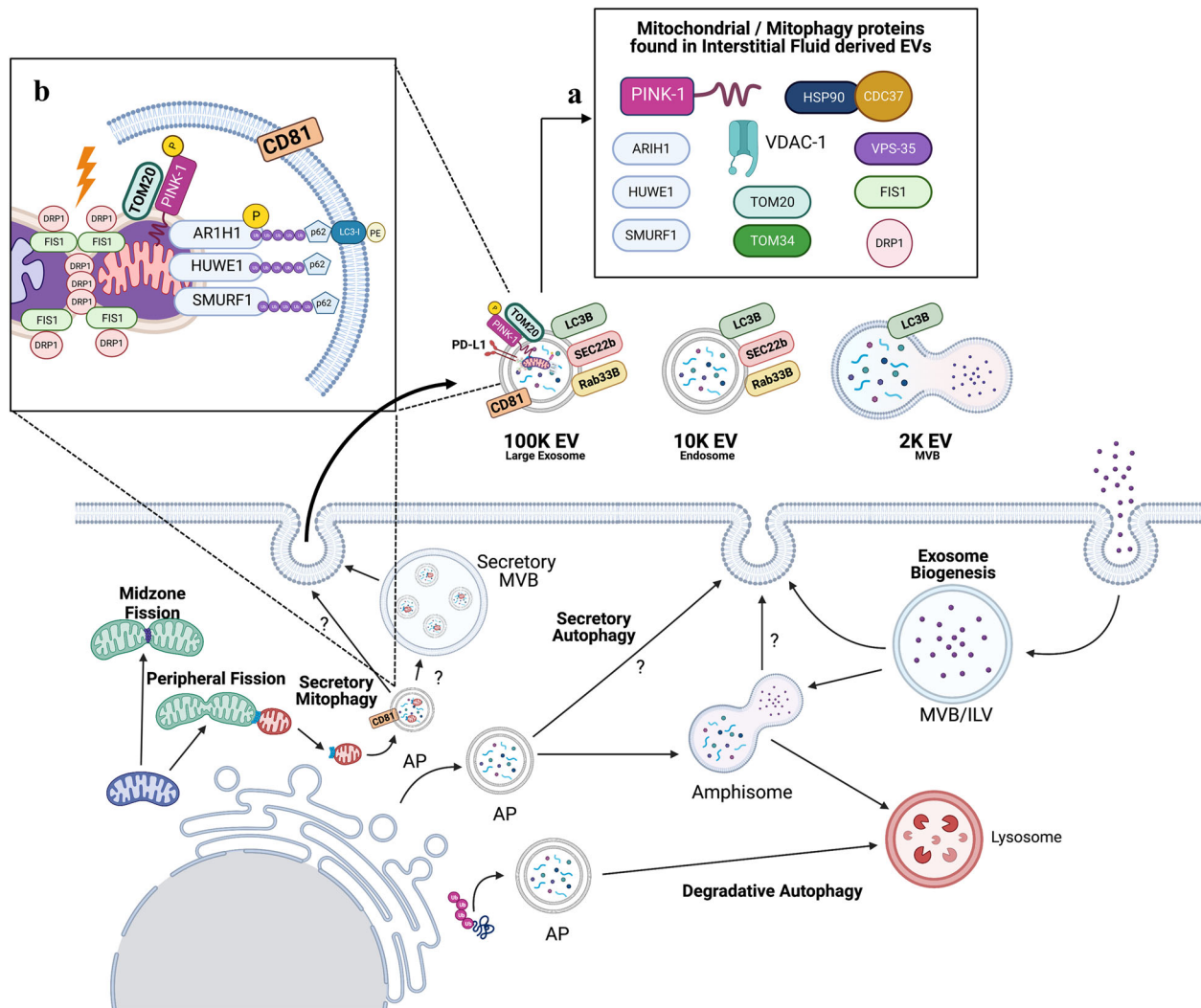


**FIGURE 8** Functional Role of EV associated Parkin-independent mitophagy-related proteins. (a) Hypothetical depiction of autophagy and mitophagy processes within the cell and their potential relation to interstitial EVs based on the results of this study. Inside the cell, unconventional protein secretion is taking place, such as secretory autophagy and mitophagy, where organelles associated with each of these types of unconventional protein secretion can be participants in the repertoire of EVs that are passively or actively secreted into the tumour or in vivo interstitium. The legend in the upper center shows the sequence-specific proteins found in high abundance in the tumour-derived 100K EVs that are related to the Parkin-independent process of mitophagy. (b) Known functional location of this complex of proteins that play in the mediation of mitophagy. EV, extracellular vesicle; AP, autophagosome; MVB, multivesicular body; ILV, intraluminal vesicle; PINK1, PTEN-induced kinase 1; DRP1, dynamin-related protein 1; FIS1, mitochondrial fission 1 protein; ARIH1, Ariadne RBR E3 Ubiquitin Protein Ligase 1; HUWE1, HECT, UBA And WWE Domain Containing E3 Ubiquitin Protein Ligase 1; SMURF1, Smad ubiquitin regulatory factor 1; Ub, ubiquitin; p62, sequestome 1; LC3, Microtubule-associated protein 1A/1B-light chain 3; PE, phosphatidylethanolamine; Sec22B, SEC22 Homolog B, Vesicle Trafficking Protein; Rab33B, Ras-Related Protein Rab-33B; HSP90/CDC37, 90 kDa heat shock protein and Cell Division Cycle 37; VDAC, Voltage dependent anion-selective channel 1 (Camara et al., 2017); TOM34, Translocase Of Outer Mitochondrial Membrane 34 (Faou and Hoogenraad, 2012); TOM20, Translocase Of Outer Mitochondrial Membrane 20 VPS-35, Vacuolar protein sorting ortholog 35

applied differential ultracentrifugation, density gradient separation, immunoprecipitation, and a variety of established methods to isolate and characterize the specific EVs (Demarino et al., 2018; Pinto et al., 2019, 2021). To our knowledge, this is the first time a breast cancer model is successfully used to isolate IF EVs from an immunocompetent animal model. We have done pilot studies to estimate reproducibility of GFP expression between tumours isolated both inter- and intra-mouse (Figure S8), and found that GFP expression is highly reproducible, indicating the EV extraction protocol is well-suited for further studies. Overall, this method is suitable for precise molecular characterization of the highly concentrated EVs shed at the tumour origin in the IF, compared to the diluted circulating tumour-derived EVs.

After qualifying and characterizing the IF EVs in vivo, we compared the protein contents of the IF EVs to cell culture-derived EVs by mass spectrometry, and functionally characterized subpopulations by immunoblotting, TEM, and endothelial tube formation analyses. Our data confirms that IF EV populations and culture-derived EV populations have many differences, as

expected. Nevertheless, they share a number of conserved protein biomarkers and multiple biologically relevant pathways that are represented consistently between both sources of EVs.

Proteomic characterization of IF fluid harvesting from different tumours, different healthy or diseased tissues, and the comparison with matched cell culture lines has to deal with vastly different total protein content. Moreover, while the proteins in IF are derived from tissue cell export and plasma filtrate, the total protein content of cell culture-derived material is dominated by FBS proteins added to the culture media. In the present study, we used EV-depleted media and adjusted culture cell densities and culture volumes for EV characterization to yield a similar range of EV particles/ml as found in the IF tumour tissue fluid (Table S2 - ZetaView Counts). We chose to normalize the samples for proteomic analysis against total volume (10  $\mu$ l) for multiple reasons. First, normalizing against total protein is inconsistent between EV subpopulations since EV subpopulations can contain different protein content per EV particle when measured by standard Bradford chemistry. Secondly, the cell culture contains FBS, which significantly alters measured protein concentration compared to tumour IF. Thirdly, the total number of tumour or host cells for a given solid tumour in contact with the IF is unknown, therefore making normalization by tumour tissue cell count difficult. Finally, the proteomic diversity of the culture compared to IF samples are vastly different due to the metabolic stress, cell cycle difference, and hypoxia placed upon the *in vivo* tumour microenvironment cells. For these reasons, important comparisons presented in Figures 3–4 between the *in vivo* IF and the culture media are normalized by volume with the goal to elucidate specific types and classes of proteins that are differentially found in the two fluid sources. For general applications of the method, it is valuable to confirm the diversity of protein identities by MS using a normalization method. To further standardize our proteomic data, we normalized our tumour IF EVs to culture-derived EVs against the total protein peptide abundance, as shown in Figure S3(a-b). We also used this same method to normalize IF samples between different tumours (Figure S3c-d). Normalization demonstrates that a comparable dynamic range of protein identities, before versus after normalization, can be achieved by the well accepted MS normalization to total peptide abundance.

As reported in Figure S4, the 4T1 model can serve as a platform to evaluate hypotheses related to lymphatic delivery of EVs to the SLN. As shown in Figure 2c we reported that IF 100K EVs are enriched for PD-L1. It has been postulated that EVs positive for PD-L1 in this same 4T1 model travel to the SLN to suppress host immune cell recognition of the upstream tumour (Poggio et al., 2019). Therefore, as a demonstration of the utility for the model, we sensitized the murine popliteal SLN by upstream injection of NPs containing immune cell chemoattractant CKs and 4T1 EV populations that accumulate in the SLN subcapsular sinus to release their cargo (Popova et al., 2015; Teunis et al., 2017). The chemoattractant draws massive numbers of immune cells including dendritic cells into the SLN to potentially overcome the PD-L1 EV suppressor function. *in vivo* syngeneic orthotopic tumour transplantation studies show that SLN preexposure of larger 2K EVs stimulates primary tumour growth and metastasis compared to suppression of tumour grow and distant metastasis by SLN pretreatment with a matching number of 100K EVs (Figure S4). A potential reason that the 2K fraction stimulates tumour growth is the content of VEGF (Figure S5 and S6) that induces vascular sprouts and angiogenesis. Further characterization of the molecular determinants for the functional differences between the pretreatment with the 2K subpopulation versus the 100K subpopulation is ongoing.

It is unclear if the immune cell priming was elicited by the presence of PD-L1 or by other 100K EV factors. Nevertheless, this model offers a potential strategy to study the role of EV subpopulations on the PD-L1+ EV cancer suppression of the SLN immune recognition of the tumour. Further investigation of this model to explore EV based cancer immunotherapy is warranted for future studies.

Our results indicated that IF EVs are numerous and have a rich content of autophagy and mitophagy specific proteins. Autophagy is a highly regulated degradative pathway that is utilized by cells to maintain homeostasis by recycling damaged, defective, misfolded, or overly abundant proteins to gain ATP in the face of hypoxia and stress. Autophagy extends to the recycling of aged or defective organelles such as mitochondria. The molecule or organelle targeted for recycling is enveloped in small double-membrane vesicles called autophagosomes. The cargo containing autophagosomes are normally shuttled to the lysosome for degradation. However, in recent years it has been documented that autophagy can function through an unconventional secretory pathway where instead of degradation at the lysosome, the autophagosomes are released through the cell membrane to enter the extracellular environment where they contribute to the repertoire of EVs. Secreted autophagosomes have been found to contain inflammatory markers such as IL-1B and IL-6 as well as whole viruses and bacteria (Dupont et al., 2011; New & Thomas, 2019). Cancer cells can increase the autophagic pathway flux as a means of survival in the face of stress (Espina et al., 2010). When the autophagic flux is too high to accommodate the limits of cellular lysosomal fusion docking sites, unconventional secretion of the autophagosomes could be a compensatory mechanism. Unconventional protein secretion (UPS) mechanisms are known to be upregulated in cancer cells to export various factors that support cancer growth, progression, and eventual metastasis. Of the four known UPS systems, EVs are secreted by cells under Type III UPS mechanisms. Type III UPS mechanisms rely on leaderless molecular intermediates such as LC3-I/II and p62 to form autophagy-related secretory vesicles (New & Thomas, 2019).

Our molecular characterization of the IF EVs show the EV-associated export of autophagy and mitophagy specific molecules released through Type III UPS mechanisms (summarized in Figure 8). Our data suggests that the EVs released by the breast cancer cells contain autophagy-related vesicular structures indicative of secretory autophagy. Based on the literature and our evidence, we hypothesize that the 2K EVs contain secretory amphisomes, which are an autophagosomes fused with late endosome/multivesicular bodies (MVB). This was supported by our TEM visualization (Figure 5c, Figure S7). The amphisome has

partially degraded autophagosome structures within (Eskelinen, 2005; Patel et al., 2013; Sanchez-Wandelmer & Reggiori, 2013). In contrast, the 100K CD81+ EVs contain non-degraded autophagy-related vesicular structures with trafficking molecules such as SEC22B and Rab33B that are associated with protein secretion rather than degradation (Table 1) (Morgan et al., 2019; New & Thomas, 2019). We hypothesize that the 100K EVs may be trafficked to the plasma membrane for release or packaged into a MVB destined for secretion.

Within the 100K EV subpopulation, we found evidence of fission mitophagy, specifically the presence of PINK1, TOM20, and E3 ubiquitin ligases which work together to drive mitophagy (Table 2, Figure 8). PINK1 is the major initiator of mitophagy and typically has been studied to initiate the E3 ubiquitin ligase Parkin to trigger the autophagy machinery to clear damaged mitochondria. Since Parkin is mainly present in neuronal cells, researchers have begun to uncover structurally similar E3 ubiquitin ligases involved in mitophagy for other cell types. Our data supports the cellular function of Parkin-independent mitophagy pathways, which use other E3 ubiquitin ligases, such as ARIH1 (Di Rita et al., 2018; Villa et al., 2017, 2018). Furthermore, Parkin-dependent mitophagy has been implicated as a noted tumour suppressor (Cesari et al., 2003; Chourasia et al., 2015; Liu et al., 2017); therefore, our findings of several Parkin-independent mitophagy intermediates secreted within tumour IF EVs represent new mechanisms of mitochondrial regulation that can potentially promote tumour growth and survival.

Cancer cells are known to use autophagy as a means to survive under hypoxia, metabolic deprivation, and treatment assaults (Espina et al., 2010). Additionally, they adapt and rewire themselves metabolically to meet the high energy and high stress demands they need to survive (MacLeod, 2020). During this transition, cancer cells may be required to cull defective or damaged mitochondria to meet these demands. In a hypoxic environment, the cell may be required to reduce the number of mitochondria within a cell to maintain oxygen levels and reduce reactive oxygen species (ROS) production. Further, the accumulation of damaged mitochondria can promote the creation of the inflammasome by the release of mitochondrial DNA which is highly deleterious to the cell (MacLeod, 2020). Under this elevated autophagic environment, the cancer cell may preferentially utilize the Type III UPS system to remove intracellular material, since endosomes, autophagosomes, and lysosomes have autophagy-related vesicular structures conserved between them (New & Thomas, 2019). Consequently, under these high stress conditions, we posit that EVs are released via secretory autophagy rather than conventional MVB endosomal release mechanisms. Ultimately, we hypothesize that cancer cells utilize EVs released from the secretory autophagy and mitophagy pathways as a means to survive intracellular stresses while also aiding the tumour by the release pro-tumour markers extracellularly. This hypothesis is supported by our results that IF EVs contain the damage associated molecular pattern (DAMP) high motility box group 1 (HGMB1) and the immune suppressor molecule PD-L1 (Table 1 - Inflammation, Angiogenesis, & Immune Activation) (Chen et al., 2018b; Zhao et al., 2018b; Othman et al., 2019; Poggio et al., 2019; Song et al., 2019; Tang et al., 2010). The concept of cell metabolic or hypoxic stress as an inducer of Parkin-independent “secretory fission mitophagy” is supported by Figure 6e-g in which induction of mitophagy by CCCP treatment or cell crowding stress was associated with an increased export of PINK1 and MitoTracker preferentially into the CD81+ 100K EV population. The augmented content of PINK1 and MitoTracker in the CD81+ EVs was not simply due to an increased total protein or total GFP labelling of EVs (Figure 7b) when the cells were under stress.

Under unstressed basal cellular conditions, PINK1 is imported into polarized mitochondria through the mitochondrial translocases of the outer and inner membranes (TOM and TIM), via the PINK1 amino-terminal mitochondrial targeting sequence (Onishi et al., 2021; Rasool et al., 2022). Following the import of PINK1, it is cleaved several times when it is in the inner mitochondrial membrane: first by the matrix processing peptidase (MPP) that removes the mitochondrial targeting sequence, with further cleavage by the inner membrane protease Presenilin-Associated Rhomboid-Like protein, generating a series of characteristic fragments (Becker et al., 2012; Choubey et al., 2022; Deas et al., 2011). Further ubiquitination and degradation of cleaved PINK1 can follow to create additional PINK1 fragments (Choubey et al., 2022). In the face of mitochondrial stress, or metabolic challenge, the corrective response can be biogenesis of more mitochondria, or excision and mitophagy of functionally impaired regions of mitochondrial. Fission of mitochondria at midzone sites is triggered by mitochondrial fission factor (MFF) and precedes mitochondrial biogenesis (Kleele et al., 2021). In contrast, fission of mitochondria at peripheral sites precedes mitochondrial mitophagy, whereby the excised region is not re-fused with healthy mitochondria, and proceeds to mitophagic breakdown. Stress induced (e.g., hypoxia, nutrient deprivation, mitochondria DNA damage) mitophagy is preferentially associated with FIS1 triggered peripheral fission, but not midzone fission (Ihenacho et al., 2021., Kleele et al., 2021). In keeping with this specific class of peripheral fission leading to mitophagy, FIS1, but not MFF, was found in the 100K IF EVs (Table 2). Under stressed and depolarized conditions, mitochondrial damage results in full length PINK1 import arrest, and arrest of full length PINK1 on the TOM complex, causing the activation of its ubiquitin kinase activity (Choubey et al., 2022). Our results (Figure S9b) clearly show that the CD81+ tumour IF EV population contains both full length PINK1 and TOM20 with matching relative abundance in all examined tumour IF samples. These findings support the conclusion that these 100K IF EVs contain mitochondria fragments derived from one or more stages of mitochondrial peripheral fission and downstream mitophagy. These experiments all point to the extracellular export of mitochondrial units of proteins associated with cellular stress and mitochondrial quality control, and that the relative abundances and fragment patterns could contain information about the metabolic state of the tumour. Although the data is highly consistent concerning their fission and mitophagy-associated content, we cannot know the exact type of EVs housing these proteins, and it is likely that there may be different types of EVs reflecting different stages of the peripheral fission triggered mitophagy cascade. It has recently been reported that whole mitochondria can be shed into the blood stream (Stephens

et al., 2020). Therefore, we cannot rule out that the export of mitophagy-associated EVs may potentially contain whole segments or fragments of mitochondria, with some fragments encased in EVs. The full definitive characterization of these EVs is ongoing. The cell export of mitochondria and mitochondrial-derived subfractions into EVs should provide a rich set of new information for future studies. These data support the hypothesis that IF tumour EVs with mitophagy specific contents are enriched because the tumour tissue is hypoxic and under metabolic stress, a known state of growing solid tumours (Onishi et al., 2021). As shown in Figure 8, the multiple mechanisms of EV release employed by the tumour cells could create distinct populations of EVs, leading to the diverse biological effects reported herein, as well as clarifying the wide range of diverse and sometimes contradictory functions assigned to tumour EVs in the literature.

This study has potential limitations. eGFP labelling of the tumour cells is not identical to the native tumour and can theoretically cause some immune recognition of the tumour beyond that for unlabelled 4T1 (Bosiljic et al., 2011). Nevertheless, as shown in Figure S4, the lymph node priming with CD81+/PINK1+ eGFP-4T1 EVs suppressed tumour growth of native 4T1 tumours, compared to SLN priming with 2K EVs, thus demonstrating the lack of a requirement for GFP tumour content for this differential response. Alternatives to GFP-expressing cell lines, such as luciferase labelled cell lines, could be used to explore labelling of IF EVs, that can extended in future studies to the trafficking of the IF EVs through the SLN and into the peripheral vascular circulation (Baklaushev et al., 2017). Our proteomic data results for specific IF EV-associated markers were observations made from one type of murine syngeneic tumour. Normalization methods for the EV IF MS data, support the reliability and reproducibility of the IF harvesting, and provide confidence that the method can be applied to any tissue or tumour type (Figure S3). Although the harvesting of IF EVs and the lack of histologic impact of the IF harvesting method on the growing solid tumour was highly reproducible in our hands, we did not study large necrotic tumours or tumours post chemotherapy. Western blot results from the MDA-MB-231 human breast cancer lines indicate similar EV and mitophagy markers present within cell-cultured EVs (Figure 6a), specifically, CD9, CD81, p62, and LC3-I/II. Density gradient separation followed by immunoprecipitation with anti-CD81 antibodies verified the presence of PINK1 in this EV gradient fraction. We did not study the IF EVs using the MDA-MB-231 cells in a human xenograft tumour model using immunosuppressed mice. Thus, we cannot separate out the role of the host immune system on the IF EV molecular composition for human tumour cells. Additional functional analyses involving inducing and suppressing autophagy and mitophagy, both in vitro and in vivo, are needed to better understand the cellular dynamics of secretory autophagy and mitophagy. Future studies exploring the specific trafficking molecules, such as Sec22B or Rab33a, that target a vesicle for secretion rather than degradation is needed. Further research is required regarding the impact of Parkin-independent mitophagy pathways and the impact of secreted (exported from living cells) mitophagy-associated EVs on cancer progression, and the value of correlating mitophagy specific PINK1 cargo in tumour resident IF EVs as a surrogate marker for tumour responses to therapy-inducing mitochondrial stress.

In summary, EVs harvested from the IF contain previously unrecognized autophagosome and mitophagy properties as well as a highly specific set of fission-mitophagy inducers and intermediates for Parkin-independent mitophagy. These secretory autophagosomes represent a potentially new biologic population of EVs that are external indicators of the metabolic state of the cell and may have a variety of important immunologic and non-immunologic functions in cancer that are associated with defective mitophagy.

## ACKNOWLEDGEMENTS

We greatly thank Andrea Brothers at American University for her imaging expertise and assistance with the TEM studies. This research study was partly supported by NIH Grants AI078859, AI074410, AI127351-01, AI043894, and NS099029 to Fatah Kashanchi, Department of Defence grant W81XWH-20-BCRP-BTA12 and NIH grants R21AI154295, R01AR068436, R33CA206937 to Lance A. Liotta, ARC Future Fellowship Award FT190100645 to Robyn P. Araujo and NIH grant R21CA251015 to Amanda Haymond.

## CONFLICT OF INTEREST

None.

## REFERENCES

- Ahsan, N. A., Sampey, G. C., Lepene, B., Akpamagbo, Y., Barclay, R. A., Iordanskiy, S., Hakami, R. M., & Kashanchi, F. (2016). Presence of viral RNA and proteins in exosomes from cellular clones resistant to rift valley fever virus infection. *Frontiers in Microbiology*, 7, 139.
- Anstine, L. J., & Keri, R. (2019). A new view of the mammary epithelial hierarchy and its implications for breast cancer initiation and metastasis. *Journal of Cancer Metastasis and Treatment*, 5, 50.
- Baklaushev, V. P., Kilpeläinen, A., Petkov, S., Abakumov, M. A., Grinenko, N. F., Yusubalieva, G. M., Latanova, A. A., Gubskiy, I. L., Zabozaev, F. G., Starodubova, E. S., Abakumova, T. O., Isagulians, M. G., & Chekhonin, V. P. (2017). Luciferase expression allows bioluminescence imaging but imposes limitations on the orthotopic mouse (4T1) model of breast cancer. *Scientific Reports*, 7, 7715.
- Becker, D., Richter, J., Tocilescu, M. A., Przedborski, S., & Voos, W. (2012). Pink1 kinase and its membrane potential ( $\Delta\psi$ )-dependent cleavage product both localize to outer mitochondrial membrane by unique targeting mode. *Journal of Biological Chemistry*, 287, 22969–22987.
- Bosiljic, M., Hamilton, M. J., Banath, J. P., Lepard, N. E., McDougal, D. C., Jia, J. X., Krystal, G., & Bennewith, K. L. (2011). Myeloid suppressor cells regulate the lung environment—Letter: Figure 1. *Cancer Research*, 71, 5050–5051.

- Braschi, E., Goyon, V., Zunino, R., Mohanty, A., Xu, L., & McBride, H. M. (2010). Vps35 Mediates Vesicle Transport between the Mitochondria and Peroxisomes. *Current Biology*, 20(14), 1310–1315.
- Camara, A. K. S., Zhou, Y., Wen, P.-C., Tajkhorshid, E., & Kwok, W.-M. (2017). Mitochondrial VDACL1: A key gatekeeper as potential therapeutic target. *Frontiers in Physiology*, 8, 460.
- Cesari, R., Martin, E. S., Calin, G. A., Pentimalli, F., Bichi, R., McAdams, H., Trapasso, F., Drusco, A., Shimizu, M., Masciullo, V., D'andrilli, G., Scambia, G., Picchio, M. C., Alder, H., Godwin, A. K., & Croce, C. M. (2003). Parkin, a gene implicated in autosomal recessive juvenile parkinsonism, is a candidate tumor suppressor gene on chromosome 6q25–q27. *PNAS*, 100, 5956–5961.
- Chazotte, B. (2011). Labeling mitochondria with mitotracker dyes. *Cold Spring Harbor Protocols*, 2011, pdbprot5648.
- Chen, C., Zhao, S., Karnad, A., & Freeman, J. W. (2018a). The biology and role of CD44 in cancer progression: Therapeutic implications. *Journal of Hematology & Oncology*, 11, 64.
- Chen, G., Huang, A. C., Zhang, W., Zhang, G., Wu, M., Xu, W., Yu, Z., Yang, J., Wang, B., Sun, H., Xia, H., Man, Q., Zhong, W., Antelo, L. F., Wu, B., Xiong, X., Liu, X., Guan, L., Li, T., ... Guo, W. (2018b). Exosomal PD-L1 contributes to immunosuppression and is associated with anti-PD-1 response. *Nature; London*, 560, 382–386.
- Chiba, M., Kubota, S., Sato, K., & Monzen, S. (2018). Exosomes released from pancreatic cancer cells enhance angiogenic activities via dynamin-dependent endocytosis in endothelial cells in vitro. *Science Reports*, 8, 1–9.
- Choubey, V., Zeb, A., & Kaasik, A. (2022). Molecular mechanisms and regulation of mammalian mitophagy. *Cells*, 11, 38.
- Chourasia, A. H., Tracy, K., Frankenberger, C., Bolland, M. L., Sharifi, M. N., Drake, L. E., Sachleben, J. R., Asara, J. M., Locasale, J. W., Karczmar, G. S., & Macleod, K. F. (2015). Mitophagy defects arising from BNIP3 loss promote mammary tumor progression to metastasis. *Embo Reports*, 16, 1145–1163.
- Cuttillo, G., Simon, D. K., & Eleuteri, S. (2020). VPS35 and the mitochondria: Connecting the dots in Parkinson's disease pathophysiology. *Neurobiology of Disease*, 145, 105056.
- Deas, E., Plun-Favreau, H., Gandhi, S., Desmond, H., Kjaer, S., Loh, S. H. Y., Renton, A. E. M., Harvey, R. J., Whitworth, A. J., Martins, L. M., Abramov, A. Y., & Wood, N. W. (2011). PINK1 cleavage at position A103 by the mitochondrial protease PARL. *Human Molecular Genetics*, 20, 867–879.
- Demarino, C., Barclay, R. A., Pleet, M. L., Pinto, D. O., Branscome, H., Paul, S., Lepene, B., El-Hage, N., & Kashanchi, F. (2019). Purification of high yield extracellular vesicle preparations away from virus. *Journal of Visualized Experiments*, 151, e59876.
- Demarino, C., Pleet, M. L., Cowen, M., Barclay, R. A., Akpamagbo, Y., Erickson, J., Ndembu, N., Charurat, M., Jumare, J., Bwala, S., Alabi, P., Hogan, M., Gupta, A., Noren Hooten, N., Evans, M. K., Lepene, B., Zhou, W., Caputi, M., Romerio, F., ... Kashanchi, F. (2018). Antiretroviral drugs alter the content of extracellular vesicles from HIV-1-infected cells. *Scientific Reports*, 8, 7653.
- De Paepe, B. (2012). Mitochondrial markers for cancer: Relevance to diagnosis, therapy, and prognosis and general understanding of malignant disease mechanisms (Hindawi).
- Di Rita, A., Peschiaroli, A., D'Acunzo, P., Strobbe, D., Hu, Z., Gruber, J., Nygaard, M., Lambrugh, M., Melino, G., Papaleo, E., Dengjel, J., El Alaoui, S., Campanella, M., Dötsch, V., Rogov, V. V., Strappazzon, F., & Cecconi, F. (2018). HUWE1 E3 ligase promotes PINK1/PARKIN-independent mitophagy by regulating AMBRA1 activation via IKK $\alpha$ . *Nature Communications*, 9, 3755.
- Dupont, N., Jiang, S., Pilli, M., Ornatowski, W., Bhattacharya, D., & Deretic, V. (2011). Autophagy-based unconventional secretory pathway for extracellular delivery of IL-1 $\beta$ . *Embo Journal*, 30, 4701–4711.
- Eskelinen, E.-L. (2005). Maturation of autophagic vacuoles in mammalian cells. *Autophagy*, 1, 1–10.
- Eskelinen, E.-L. (2008). To be or not to be? Examples of incorrect identification of autophagic compartments in conventional transmission electron microscopy of mammalian cells. *Autophagy*, 4, 257–260.
- Espina, V., Edmiston, K. H., Heiby, M., Pierobon, M., Sciro, M., Merritt, B., Banks, S., Deng, J., VanMeter, A. J., Geho, D. H., Pastore, L., Sennesh, J., & Petricoin, E. F. 3rd. (2008). A portrait of tissue phosphoprotein stability in the clinical tissue procurement process. *Molecular & Cellular Proteomics*, 7, 1998–2018.
- Espina, V., Mariani, B. D., Gallagher, R. I., Tran, K., Banks, S., Wiedemann, J., Huryk, H., Mueller, C., Adamo, L., Deng, J., Petricoin, E. F., Pastore, L., Zaman, S., Menezes, G., Mize, J., Johal, J., Edmiston, K., & Liotta, L. A. (2010). Malignant precursor cells pre-exist in human breast DCIS and require autophagy for survival. *Plos One*, 5, e10240.
- Faou, P., & Hoogenraad, N. J. (2012). Tom34: A cytosolic cochaperone of the Hsp90/Hsp70 protein complex involved in mitochondrial protein import. *Biochimica et Biophysica Acta (BBA) - Molecular Cell Research*, 1823, 348–357.
- Fleming, A., Sampey, G., Chung, M.-C., Bailey, C., Van Hoek, M. L., Kashanchi, F., & Hakami, R. M. (2014). The carrying pigeons of the cell: Exosomes and their role in infectious diseases caused by human pathogens. *Pathogens and Disease*, 71, 109–120.
- Gallart-Palau, X., Serra, A., & Sze, S. K. (2016). Enrichment of extracellular vesicles from tissues of the central nervous system by PROSPR. *Molecular Neurodegeneration*, 11, 41.
- Groza, M., Zimta, A. - A., Irimie, A., Achimas-Cadariu, P., Cenariu, D., Stanta, G., & Berindan-Neagoe, I. (2020). Recent advancements in the study of breast cancer exosomes as mediators of intratumoral communication. *Journal of Cellular Physiology*, 235(2), 691–705.
- Heberle, H., Meirelles, G. V., Da Silva, F. R., Telles, G. P., & Minghim, R. (2015). InteractiVenn: A web-based tool for the analysis of sets through Venn diagrams. *Bmc Bioinformatics [Electronic Resource]*, 16, 169.
- Ihenacho, U. K., Meacham, K. A., Harwig, M. C., Widlansky, M. E., & Hill, R. B. (2021). Mitochondrial fission protein 1: Emerging roles in organellar form and function in health and disease. *Frontiers in Endocrinology*, 12, 660095.
- Jang, S. C., Crescitelli, R., Cvjetkovic, A., Belgrano, V., Olofsson Bagge, R., Sundfeldt, K., Ochiya, T., Kalluri, R., & Lötval, J. (2019). Mitochondrial protein enriched extracellular vesicles discovered in human melanoma tissues can be detected in patient plasma. *Journal of Extracellular Vesicles*, 8, 1635420.
- Jung, M. K., & Mun, J. Y. (2018). Sample preparation and imaging of exosomes by transmission electron microscopy. *Journal of Visualized Experiments*, 131, e56482.
- Katsuragi, Y., Ichimura, Y., & Komatsu, M. (2015). p62/SQSTM1 functions as a signaling hub and an autophagy adaptor. *The FEBS Journal*, 282, 4672–4678.
- Kleele, T., Rey, T., Winter, J., Zaganelli, S., Mahecic, D., Perreten Lambert, H., Ruberto, F. P., Nemir, M., Wai, T., Pedrazzini, T., & Manley, S. (2021). Distinct fission signatures predict mitochondrial degradation or biogenesis. *Nature*, 593, 435–439.
- Leblanc, M. E., Wang, W., Caberoy, N. B., Chen, X., Guo, F., Alvarado, G., Shen, C., Wang, F., Wang, H., Chen, R., Liu, Z.-J., Webster, K., & Li, W. (2015). Hepatoma-derived growth factor-related protein-3 is a novel angiogenic factor. *Plos One*, 10, e0127904.
- Liu, J., Zhang, C., Zhao, Y., Yue, X., Wu, H., Huang, S., Chen, J., Tomsy, K., Xie, H., Khella, C. A., Gatz, M. L., Xia, D., Gao, J., White, E., Haffty, B. G., Hu, W., & Feng, Z. (2017). Parkin targets HIF-1 $\alpha$  for ubiquitination and degradation to inhibit breast tumor progression. *Nature Communications*, 8, 1823.
- Liu, T., Han, C., Wang, S., Fang, P., Ma, Z., Xu, L., & Yin, R. (2019). Cancer-associated fibroblasts: An emerging target of anti-cancer immunotherapy. *Journal of Hematology & Oncology*, 12, 86.
- Liu, W., & Hajjar, K. A. (2016). The annexin A2 system and angiogenesis. *Biological Chemistry*, 397, 1005–1016.

- Longo, C., Patanarut, A., George, T., Bishop, B., Zhou, W., Fredolini, C., Ross, M. M., Espina, V., Pellacani, G., Petricoin, E. F., Liotta, L. A., & Luchini, A. (2009). Core-shell hydrogel particles harvest, concentrate and preserve labile low abundance biomarkers. *Plos One*, *4*, e4763.
- Lowry, M. C., Gallagher, W. M., & O'driscoll, L. (2015). The role of exosomes in breast cancer. *Clinical Chemistry*, *61*, 1457–1465.
- Luchini, A., Geho, D. H., Bishop, B., Tran, D., Xia, C., Dufour, R. L., Jones, C. D., Espina, V., Patanarut, A., Zhou, W., Ross, M. M., Tessitore, A., Petricoin, E. F., & Liotta, L. A. (2008). Smart hydrogel particles: Biomarker harvesting: one-step affinity purification, size exclusion, and protection against degradation. *Nano Letters*, *8*, 350–361.
- Macleod, K. F. (2020). Mitophagy and mitochondrial dysfunction in cancer. *Annual Review of Cancer Biology*, *4*, 41–60.
- Madu, C. O., Wang, S., Madu, C. O., & Lu, Y. (2020). Angiogenesis in breast cancer progression, diagnosis, and treatment. *Journal of Cancer*, *11*, 4474–4494.
- Magni, R., Almofoee, R., Yusuf, S., Mueller, C., Vuong, N., Almosuli, M., Hoang, M. T., Meade, K., Sethi, I., Mohammed, N., Araujo, R., McDonald, T. K., Marcelli, P., Espina, V., Kim, B., Garritsen, A., Green, C., Russo, P., Zhou, W., ... Luchini, A. (2020). Evaluation of pathogen specific urinary peptides in tick-borne illnesses. *Science Reports*, *10*, 19340.
- Maji, S., Chaudhary, P., Akopova, I., Nguyen, P. M., Hare, R. J., Gryczynski, I., & Vishwanatha, J. K. (2017). Exosomal annexin II promotes angiogenesis and breast cancer metastasis. *Molecular Cancer Research*, *15*, 93–105.
- Margolis, L., & Sadovsky, Y. (2019). The biology of extracellular vesicles: The known unknowns. *PLOS Biology*, *17*, e3000363.
- Mashouri, L., Yousefi, H., Aref, A. R., Ahadi, A. M., Molaei, F., & Alahari, S. K. (2019). Exosomes: Composition, biogenesis, and mechanisms in cancer metastasis and drug resistance. *Molecular Cancer*, *18*, 75.
- Melino, G., Ceconi, F., Pelicci, P. G., Mak, T. W., & Bernassola, F. (2019). Emerging roles of HECT-type E3 ubiquitin ligases in autophagy regulation. *Molecular Oncology*, *13*, 2033–2048.
- Menz, A., Weitbrecht, T., Gorbokov, N., BÄ¼Scheck, F., Luecke, A. M., Kluth, M., Hube-Magg, C., Hinsch, A., Höflmayer, D., Weidemann, S., Fraune, C., Möller, K., Bernreuther, C., Lebok, P., Clauditz, T., Sauter, G., Uhlig, R., Wilczak, W., Steurer, S., ... Simon, R. (2021). Diagnostic and prognostic impact of cytokeratin 18 expression in human tumors: A tissue microarray study on 11,952 tumors. *Molecular Medicine*, *27*, 16.
- Mi, H., & Thomas, P. (2009). PANTHER Pathway: An ontology-based pathway database coupled with data analysis tools. *Methods in Molecular Biology*, *563*, 123–140.
- Mincheva-Nilsson, L., Baranov, V., Nagaeva, O., & Dehlin, E. (2016). Isolation and characterization of exosomes from cultures of tissue explants and cell lines. *Current Protocols in Immunology*, *115*, 14.42.1–14.42.21.
- Mizushima, N., & Yoshimori, T. (2007). How to Interpret LC3 Immunoblotting. *Autophagy*, *3*(6), 542–545.
- Morgan, N. E., Cutrona, M. B., & Simpson, J. C. (2019). Multitasking Rab proteins in autophagy and membrane trafficking: A focus on Rab33b. *International Journal of Molecular Sciences*, *20*, 3916.
- Muller, L., Mitsuhashi, M., Simms, P., Gooding, W. E., & Whiteside, T. L. (2016). Tumor-derived exosomes regulate expression of immune function-related genes in human T cell subsets. *Science Reports*, *6*, 20254.
- Narayanan, A., Iordanskiy, S., Das, R., Van Duyne, R., Santos, S., Jaworski, E., Guendel, I., Sampey, G., Dalby, E., Iglesias-Ussel, M., Popratiloff, A., Hakami, R., Kehn-Hall, K., Young, M., Subra, C., Gilbert, C., Bailey, C., Romero, F., & Kashanchi, F. (2013). Exosomes derived from HIV-1-infected cells contain trans-activation response element RNA. *Journal of Biological Chemistry*, *288*, 20014–20033.
- New, J., & Thomas, S. M. (2019). Autophagy-dependent secretion: Mechanism, factors secreted, and disease implications. *Autophagy*, *15*, 1682–1693.
- Onishi, M., Yamano, K., Sato, M., Matsuda, N., & Okamoto, K. (2021). Molecular mechanisms and physiological functions of mitophagy. *Embo Journal*, *40*, e104705.
- Othman, N., Jamal, R., & Abu, N. (2019). Cancer-derived exosomes as effectors of Ke inflammation-related players. *Frontiers in Immunology*, *10*, 2103.
- Patel, K. K., Miyoshi, H., Beatty, W. L., Head, R. D., Malvin, N. P., Cadwell, K., Guan, J.-L., Saitoh, T., Akira, S., Seglen, P. O., Dinauer, M. C., Virgin, H. W., & Stappenbeck, T. S. (2013). Autophagy proteins control goblet cell function by potentiating reactive oxygen species production. *Embo Journal*, *32*, 3130–3144.
- Pinto, D. O., Al Sharif, S., Mensah, G., Cowen, M., Khatkar, P., Erickson, J., Branscome, H., Lattanze, T., Demarino, C., Alem, F., Magni, R., Zhou, W., Alais, S., Dutartre, H., El-Hage, N., Mahieux, R., Liotta, L. A., & Kashanchi, F. (2021). Extracellular vesicles from HTLV-1 infected cells modulate target cells and viral spread. *Retrovirology*, *18*, 6.
- Pinto, D. O., Demarino, C., Pleet, M. L., Cowen, M., Branscome, H., Al Sharif, S., Jones, J., Dutartre, H., Lepene, B., Liotta, L. A., Mahieux, R., & Kashanchi, F. (2019). HTLV-1 extracellular vesicles promote cell-to-cell contact. *Frontiers in microbiology*, *10*, 2147.
- Pircher, A., Hilbe, W., Heidegger, I., Drevs, J., Tichelli, A., & Medinger, M. (2011). Biomarkers in tumor angiogenesis and anti-angiogenic therapy. *International Journal of Molecular Sciences*, *12*, 7077–7099.
- Pleet, M. L., Branscome, H., Demarino, C., Pinto, D. O., Zadeh, M. A., Rodriguez, M., Sariyer, I. K., El-Hage, N., & Kashanchi, F. (2018). Autophagy, EVs, and infections: A perfect question for a perfect time. *Frontiers in Cellular and Infection Microbiology*, *8*, 362.
- Pleet, M. L., Mathiesen, A., Demarino, C., Akpamagbo, Y. A., Barclay, R. A., Schwab, A., Iordanskiy, S., Sampey, G. C., Lepene, B., Ilinykh, P. A., Bukreyev, A., Nekhai, S., Aman, M. J., & Kashanchi, F. (2016). Ebola VP40 in exosomes can cause immune cell dysfunction. *Frontiers in Microbiology*, *7*, 1765.
- Poggio, M., Hu, T., Pai, C.-C., Chu, B., Belair, C. D., Chang, A., Montabana, E., Lang, U. E., Fu, Q., Fong, L., & Billelo, R. (2019). Suppression of exosomal PD-L1 induces systemic anti-tumor immunity and memory. *Cell*, *177*, 414–427.e13.
- Popova, T., Teunis, A., Magni, R., Luchini, A., Espina, V., Liotta, L., & Popov, S. (2015). Chemokine-releasing nanoparticles for manipulation of lymph node microenvironment. *Nanomaterials (Basel)*, *5*, 298–320.
- Pulaski, B. A., & Ostrand-Rosenberg, S. (2000). Mouse 4T1 breast tumor model. *Current Protocols in Immunology*, *39*, 20.2.1–20.2.16.
- Raposo, G., & Stoorvogel, W. (2013). Extracellular vesicles: Exosomes, microvesicles, and friends. *Journal of Cell Biology*, *200*, 373–383.
- Rasool, S., Veyron, S., Soya, N., Eldeeb, M. A., Lukacs, G. L., Fon, E. A., & Trempe, J.-F. (2022). Mechanism of PINK1 activation by autophosphorylation and insights into assembly on the TOM complex. *Molecular Cell*, *82*, 44–59.e6.
- Roberts, R. F., Tang, M. Y., Fon, E. A., & Durcan, T. M. (2016). Defending the mitochondria: The pathways of mitophagy and mitochondrial-derived vesicles. *The International Journal of Biochemistry & Cell Biology*, *79*, 427–436.
- Sampey, G. C., Saifuddin, M., Schwab, A., Barclay, R., Punya, S., Chung, M.-C., Hakami, R. M., Asad Zadeh, M., Lepene, B., Klase, Z. A., El-Hage, N., Young, M., Iordanskiy, S., & Kashanchi, F. (2016). Exosomes from HIV-1-infected cells stimulate production of pro-inflammatory cytokines through trans-activating Response (TAR) RNA. *Journal of Biological Chemistry*, *291*, 1251–1266.
- Sanchez-Wandelmer, J., & Reggiori, F. (2013). Amphisomes: Out of the autophagosome shadow? *Embo Journal*, *32*, 3116–3118.
- Song, Y., Wu, L., & Yang, C. (2019). Exosomal PD-L1: An effective liquid biopsy target to predict immunotherapy response. *National Science Review*, *6*, 1103–1104.
- Stacker, S. A., Williams, S. P., Karnezis, T., Shayan, R., Fox, S. B., & Achen, M. G. (2014). Lymphangiogenesis and lymphatic vessel remodelling in cancer. *Nature Reviews Cancer*, *14*, 159–172.

- Stephens, O. R., Grant, D., Frimel, M., Wanner, N., Yin, M., Willard, B., Erzurum, S. C., & Asosingh, K. (2020). Characterization and origins of cell-free mitochondria in healthy murine and human blood. *Mitochondrion*, *54*, 102–112.
- Sun, A., Wei, J., Childress, C., Shaw, J. H., Peng, K., Shao, G., Yang, W., & Lin, Q. (2017). The E3 ubiquitin ligase NEDD4 is an LC3-interactive protein and regulates autophagy. *Autophagy*, *13*(3), 522–537.
- Tamburro, D., Fredolini, C., Espina, V., Douglas, T. A., Ranganathan, A., Ilag, L., Zhou, W., Russo, P., Espina, B. H., Muto, G., Petricoin, E. F., Liotta, L. A., & Luchini, A. (2011). Multifunctional core-shell nanoparticles: Discovery of previously invisible biomarkers. *Journal of the American Chemical Society*, *133*, 19178–19188.
- Tang, D., Kang, R., Zeh Iii, H. J., & Lotze, M. T. (2010). High-mobility Group Box 1 [HMGB1] and cancer. *Biochimica et Biophysica Acta*, *1799*, 131.
- Teng, Y., Ren, Y., Hu, X., Mu, J., Samykutty, A., Zhuang, X., Deng, Z., Kumar, A., Zhang, L., Merchant, M. L., Yan, J., Miller, D. M., & Zhang, H.-G. (2017). MVP-mediated exosomal sorting of miR-193a promotes colon cancer progression. *Nature Communications*, *8*, 14448.
- Teunis, A. L., Popova, T. G., Espina, V., Liotta, L. A., & Popov, S. G. (2017). Immune-modulating activity of hydrogel microparticles contributes to the host defense in a murine model of cutaneous anthrax. *Frontiers in Molecular Biosciences*, *4*, 62.
- Thomas, S. N., Vokali, E., Lund, A. W., Hubbell, J. A., & Swartz, M. A. (2014). Targeting the tumor-draining lymph node with adjuvanted nanoparticles reshapes the anti-tumor immune response. *Biomaterials*, *35*, 814–824.
- Vader, P., Breakefield, X. O., & Wood, M. J. A. (2014). Extracellular vesicles: Emerging targets for cancer therapy. *Trends in Molecular Medicine*, *20*, 385–393.
- Vella, L. J., Scicluna, B. J., Cheng, L., Bawden, E. G., Masters, C. L., Ang, C.-S., Williamson, N., Mclean, C., Barnham, K. J., & Hill, A. F. (2017). A rigorous method to enrich for exosomes from brain tissue. *Journal of Extracellular Vesicles*, *6*, 1348885.
- Villa, E., Marchetti, S., & Ricci, J.-E. (2018). No Parkin zone: Mitophagy without parkin. *Trends in Cell Biology*, *28*, 882–895.
- Villa, E., Proïcs, E., Rubio-Patiño, C., Obba, S., Zunino, B., Bossowski, J. P., Rozier, R. M., Chiche, J., Mondragá<sup>3</sup>N, L., Riley, J. S., Marchetti, S., Verhoeven, E., Tait, S. W. G., & Ricci, J.-E. (2017). Parkin-independent mitophagy controls chemotherapeutic response in cancer cells. *Cell Reports*, *20*, 2846–2859.
- Vlassov, A. V., Magdaleno, S., Setterquist, R., & Conrad, R. (2012). Exosomes: current knowledge of their composition, biological functions, and diagnostic and therapeutic potentials. *Biochimica et Biophysica Acta*, *1820*, 940–948.
- Wang, J., Davis, S., Zhu, M., Miller, E. A., & Ferro-Novick, S. (2017). Autophagosome formation: Where the secretory and autophagy pathways meet. *Autophagy*, *13*, 973–974.
- Xi, L., Peng, M., Liu, S., Liu, Y., Wan, X., Hou, Y., Qin, Y., Yang, L., Chen, S., Zeng, H., Teng, Y., Cui, X., & Liu, M. (2021). Hypoxia-stimulated ATM activation regulates autophagy-associated exosome release from cancer-associated fibroblasts to promote cancer cell invasion. *Journal of Extracellular Vesicles*, *10*, e12146.
- Yadav, B. S. (2015). Biomarkers in triple negative breast cancer: A review. *World journal of clinical oncology*, *6*, 252–263.
- Yoon, Y., Krueger, E. W., Oswald, B. J., & Mcniven, M. A. (2003). The mitochondrial protein hfs1 regulates mitochondrial fission in mammalian cells through an interaction with the dynamin-like protein DLP1. *Molecular and Cellular Biology*, *23*, 5409–5420.
- Yoshii, S. R., & Mizushima, N. (2017). Monitoring and measuring autophagy. *International Journal of Molecular Sciences*, *18*, 1865.

## SUPPORTING INFORMATION

Additional supporting information can be found online in the Supporting Information section at the end of this article.

**How to cite this article:** Howard, M., Erickson, J., Cuba, Z., Kim, S., Zhou, W., Gade, P., Carter, R., Mitchell, K., Branscome, H., Siddhi, D., Alanazi, F., Kim, Y., Araujo, R. P., Haymond, A., Luchini, A., Kashanchi, F., & Liotta, L. A. (2022). A secretory form of Parkin-independent mitophagy contributes to the repertoire of extracellular vesicles released into the tumour interstitial fluid in vivo. *Journal of Extracellular Vesicles*, *11*, e12244. <https://doi.org/10.1002/jev2.12244>